Cite this article
Macedo J, Torres P, Vergaray L, Paihua S and Arnold C (2022)
Dynamic effective stress analysis of a centreline tailings dam under subduction earthquakes.
Proceedings of the Institution of Civil Engineers – Geotechnical Engineering **175(2)**: 224–246,
https://doi.org/10.1680/jgeen.21.00017a

Research Article
Paper 2100017a
Received 14/03/2021;
Accepted 26/01/2022;
Published online 16/02/2022

Geotechnical Engineering

ice Publishing

Dynamic effective stress analysis of a centreline tailings dam under subduction earthquakes

Jorge Macedo PhD
Assistant Professor, Georgia Institute of Technology, Atlanta, GA, USA
(corresponding author: jorge.macedo@gatech.edu)

Paola Torres BSc
Engineer II, Knight Piésold Consultores, Lima, Lima, Peru

Luis Vergaray MSc
PhD candidate, Georgia Institute of Technology, Atlanta, GA, USA

Solange Paihua MSc
Senior Geotechnical Engineer, Knight Piésold Consultores, Lima, Lima, Peru

Cody Arnold MSc
PhD candidate, Georgia Institute of Technology, Atlanta, GA, USA

A case study was conducted to evaluate the seismic performance of a centreline tailings dam in the South American Andes through dynamic effective stress analyses with advanced constitutive models. The seismic demand at the dam site was evaluated through a probabilistic seismic hazard assessment (PSHA), from which deterministic and probabilistic-based seismic design criteria were derived. The PSHA results were used to select spectrally matched ground motions for the subsequent dynamic analyses. The plan is for the centreline tailings dam to be raised in stages to a height of 90 m; this was considered in establishing the initial stresses and pore pressures before seismic loading. The material properties were based on a large geotechnical characterisation programme considering the mine tailings to be stored in the deposit and other critical dam components. Dynamic analyses were performed using the UBCHYST constitutive model for materials that are not expected to generate significant excess pore pressures and the PM4Silt constitutive model for materials that may generate excess pore pressures due to cyclic loading. The results showed the deformation patterns in the centreline dam, after seismic loading, to be significantly affected by the presence of mine tailings. The results of this work will be useful in planning the overall operational management of the tailings facility.

Keywords: dams, barrages & reservoirs/geotechnical engineering/mining & environmental issues/seismic engineering/tailings

Notation

e	void ratio
G	shear modulus
G/G_{max}	normalised shear modulus
G_{max}	maximum shear modulus
G_s	specific gravity
G_t	tangent shear modulus
G_0	shear modulus coefficient
h_{p0}	contraction rate parameter
K_σ	overburden stress correction factor for liquefaction triggering
$k_{2,max}$	modulus coefficient
M_{tc}	critical state friction ratio
M_w	moment magnitude
$n_{b,wet}$, $n_{b,dry}$	bounding surface parameters
n_G	shear modulus exponent
P_a	atmospheric pressure
p'	mean effective stress
p_{cs}	mean effective stress at critical state
R_u	excess pore pressure ratio
S_u/σ'_{vc}	normalised shear strength
$S_{u,cs}$	ultimate shear strength
$S_{u,cs}/\sigma'_{vc}$	ultimate shear strength ratio
T_s	spectral period
V_s	shear wave velocity
Γ	altitude of critical state line (CSL)
γ	horizontal shear strain
Δu	excess pore pressure
$\Delta\phi$	friction angle reduction for every log cycle of stress level increase
η	current stress ratio ($= \tau_{xy}/\sigma'_v$,)
η_{max}	maximum stress ratio at last reversal
η_1	change in stress ratio since the last reversal ($= \eta - \eta_{max}$)
η_{1f}	change in stress ratio to reach the failure envelope ($= \eta_f - \eta_{max}$)
λ	slope of CSL
ρ	density of material
ρ_d	dry density
σ'_v	vertical effective stress
σ'_{v0}	initial vertical effective stress
σ'_{vc}	vertical effective stress after consolidation
τ_{xy}	shear stress
ϕ	friction angle
ϕ_{cv}	critical state friction angle
ϕ_1	reference friction angle

1. Introduction

Non-linear dynamic effective stress analysis of a centreline tailings dam located in the South American Andes is presented. The dam is located in a region of high-seismicity, known as

the Pacific Ring of Fire. On a larger scale, the regional tectonic framework is governed by the interaction of the Nazca and South American plates. The border between these plates in this region is demarcated by the Peru–Chile trench. The continuous subduction of the Nazca plate along the Peru–Chile trench is the primary source of large earthquakes ($M_w > 7.0$).

The centreline construction method was selected to build the dam, which is part of a tailings storage facility (TSF), as this method optimises the available storage while minimising the required volume of construction materials. The dam will retain tailings during operation and after closure. It will have a height of 90 m and its crest length will be approximately 560 m. The dam will be built in six stages, considering a starter dam and five sequential centrelined raisings supported by an upstream rockfill platform. For the starter dam and raisings, the downstream slopes are 2H:1.0V and 2.3H:1.0V, respectively, whereas the upstream slopes are 1.7H:1.0V and 1.5H:1.0V. The analyses presented in this article were conducted to evaluate the seismic response of the dam, which is controlled by the patterns seen in seismically induced deformations when design ground motions shake the dam.

The current state of practice in the seismic assessment of tailings dams uses several simplified procedures, which are more suitable for tailings dams built using the downstream method (e.g. Bray *et al.*, 2018; Bray and Macedo, 2019; Macedo *et al.*, 2017; Macedo *et al.*, 2020; Macedo and Candia, 2020). However, when potentially liquefiable materials influence the seismic performance of a tailings dam (as is the case discussed here), more rigorous procedures should be employed. In the context of this study, the seismic response of the tailings dam is strongly dependent on the seismic response of the mine tailings that will be stored. Advanced laboratory tests (static, cyclic and dynamic) were thus performed to characterise the mine tailings to be deposited. The laboratory tests revealed interesting insights into the mechanical response of the mine tailings, which were used to calibrate an advanced numerical model and to treat the seismic response of the tailings dam as a boundary value problem. The aim of this study was to illustrate the current state of the art in the seismic assessment of centreline tailings dams as part of the geotechnical earthquake engineering practice within the mining industry. As discussed by Boulanger and Ziotopoulou (2018a), the use of non-linear dynamic effective stress analysis for assessing the seismic response of dam systems in engineering practice has gained relevance – as such, this and other case studies are crucial in helping to further best practices.

2. Description of the dam, foundation and tailings materials

The information collected from geotechnical site investigations was reviewed and interpreted to characterise the dam, foundation and tailings materials. The dam considered in this study has not yet been built; therefore, some material properties were estimated based on laboratory tests performed on samples obtained from quarries and tailings samples obtained from a pilot processing plant. The foundation properties were estimated based on field tests (e.g. permeability and geophysical tests). The dam will mainly be composed of structural fill, a core, filter/drain and a rockfill platform (Figure 1). The structural fill and core are to consist of till materials (clayey gravel), with the core materials having a plasticity index (PI) generally larger than 15 and the fill having no plasticity. The filter/drain will comprise coarse and medium sand, while the rockfill platform material is mainly cobbles and boulders. The starter dam also includes an upstream geomembrane to prevent contact water from entering the dam body. The foundation comprises two groups of rocks belonging to the Ambo and Copacabana

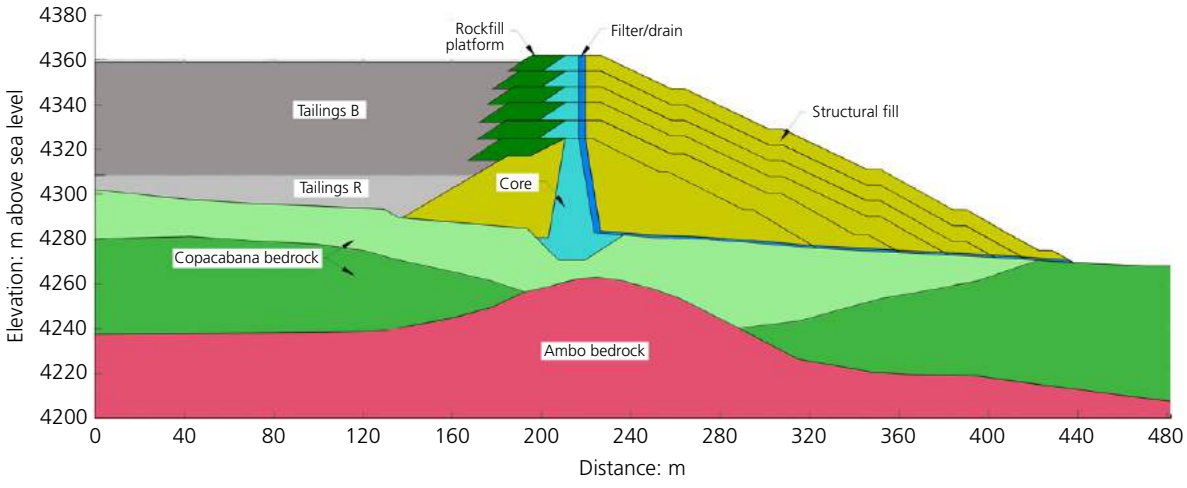

Figure 1. Cross-section of the centreline dam

geological groups. The Ambo group has a presence of sandstones with thin horizons of siltstone and bituminous shales. This rock is moderately weathered, of low to medium strength and is slightly to moderately fractured. The Copacabana group comprises limestone rocks with intercalations of dolomite horizons, calcareous breccia, calcareous sandstone and siltstone. The upper stratum of this group is moderate to highly weathered, of low strength and moderately to very fractured, while the lower stratum is slight to moderately weathered, of medium to high strength and slightly to moderately fractured. Two types of tailings, denominated tailings R and B, will be stored in the tailings facility and were characterised as part of this study. Tailings R is silty clay with a low to medium PI (= 9), 98% fines content (FC) and an average specific gravity (G_s) of 2.8. Tailings B is sandy silt, with an average FC of 65%, a PI lower than 4 and $G_s = 2.81$. Figure 1 shows the cross-section of the dam and the different materials. Figure 2 shows the particle size distribution of the mine tailings and other materials in the dam.

3. Seismic design criteria and ground motions

The seismic demand at the dam location was evaluated through a probabilistic seismic hazard assessment (PSHA) considering the contribution of the subduction interface, subduction intraslab and shallow crustal seismic sources in the platform SeismicHazard (Candia *et al.*, 2018, 2019). Figure 3(a) shows the different seismic sources contributing to the seismic hazard at the dam site, Figure 3(b) shows the hazard curves for different spectral periods ($T_s = 0$, 0.2 and 1.0 s), Figure 3(c) shows the uniform hazard spectra for different return periods and Figure 3(d) shows the deterministic response spectra calculated using the dominant earthquake scenario, which corresponds to an earthquake of magnitude 8.0 at 160 km from the dam site, in the upper intraslab seismic source. Using the Canadian Dam Association's dam safety guidelines (CDA, 2014), the seismic risk associated with the dam was classified as 'extreme'. These guidelines recommend the so-called maximum credible earthquake (MCE) or ground motions with a return of 10 000 years for extreme hazard dams. However, following the guidelines of Martinez and Hull (2019), which are consistent with conventional practice in South America, the design earthquake was defined as the 84th percentile of the deterministic analysis and ultimately used for selecting the design ground motions (see Section 8 for further details). The resulting peak horizontal ground acceleration (PGA) for the MCE is 0.34***g***, as shown in Figure 3(d). Of note, the Pacific Earthquake Engineering Research Center has recently released new ground motion models for subduction zones (Bozorgnia *et al.*, 2021). These models were not considered in this study, but their performance for the South American Andes should be carefully assessed in future research.

The focus of the dynamic analyses (discussed in the following sections) was on evaluating the mean response of engineering demand parameters of interest in the dam (e.g. seismically induced displacements). Thus, the spectral matching method (Al Atik and Abrahamson, 2010) was used to generate design ground motions consistent with the deterministic design spectrum. Consistent with the common practice in South America, five time histories were generated, three of which were used in the subsequent effective stress dynamic analyses. Figure 4

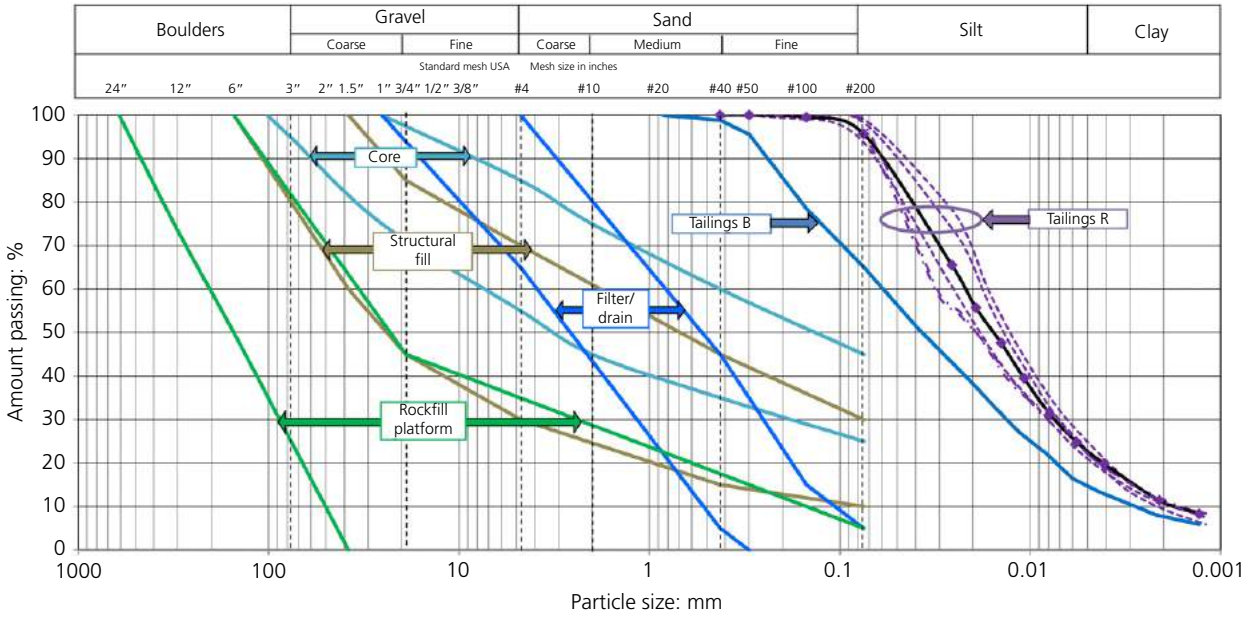

Figure 2. Particle size distributions of mine tailings and dam materials (1 inch = 2.54 cm)

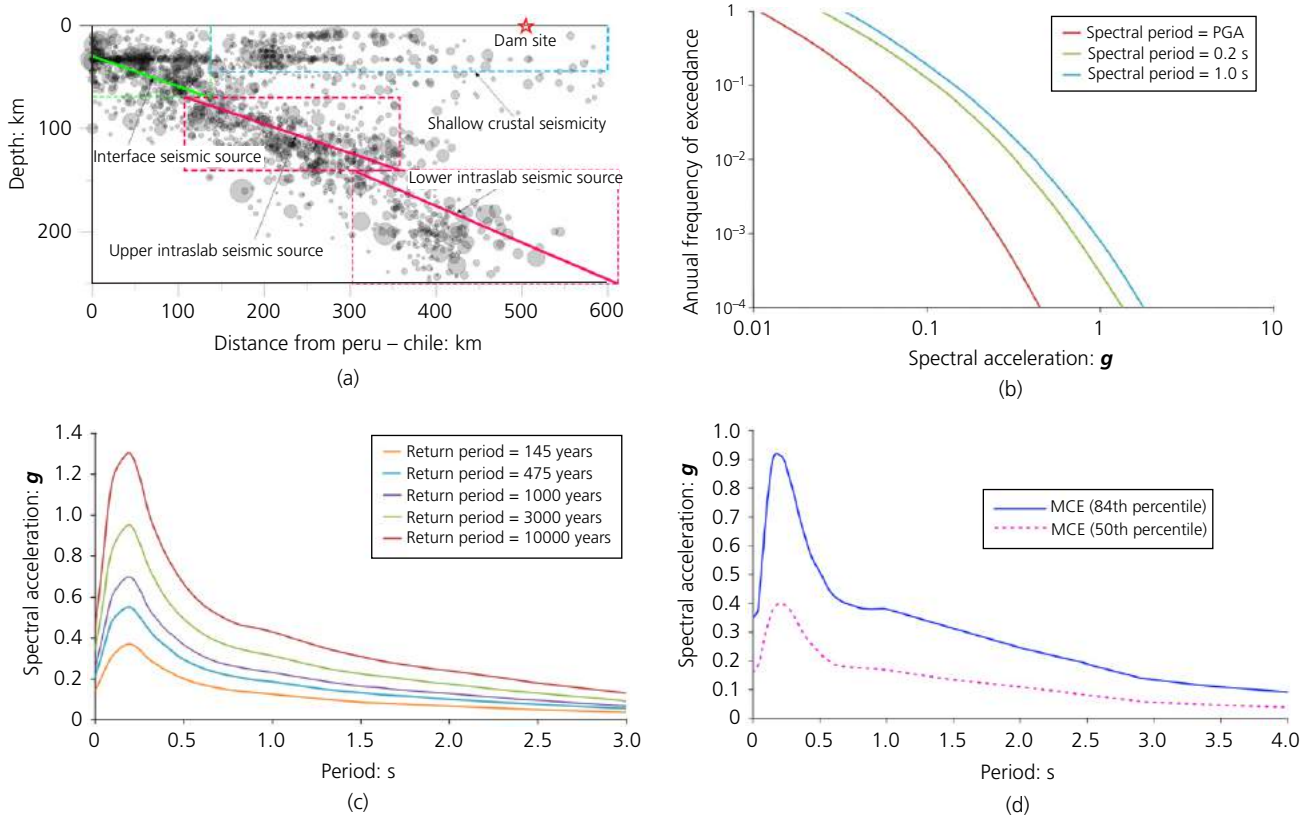

Figure 3. (a) Seismic sources affecting the dam; (b) hazard curves; (c) uniform hazard spectra; (d) deterministic MCE response spectra (50th and 84th percentiles)

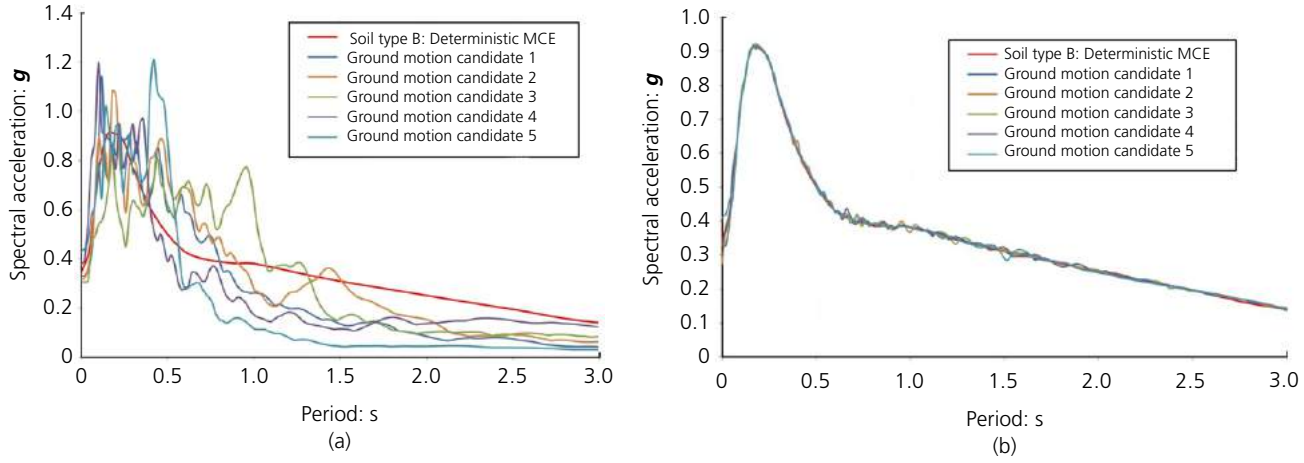

Figure 4. Response spectra of ground motions spectrally matched to the design spectrum: (a) original ground motion; (b) spectrally matched ground motions

shows a comparison of the deterministic design spectrum (i.e. 84th percentile) and the spectrally matched ground motion records.

4. Geotechnical characterisation

Given the importance of the mine tailings' mechanical response on the dam's seismic performance (see Figure 1), a

detailed characterisation of the response of the two mine tailings to be deposited was undertaken. As noted by Macedo and Vergaray (2021) and further discussed in this article, mine tailings often have a distinctive response and therefore should be properly characterised. In addition, resonant column tests were performed on materials representative of the dam core, given its importance on the overall seismic response of the dam. In the laboratory, cyclic simple shear (CSS) tests, consolidated undrained and drained triaxial tests (CUTX and CDTX, respectively), monotonic simple shear (DSS) tests and bender element (BE) tests were conducted on the two types of tailings. In addition, resonant column tests were conducted on tailings B.

Figure 5 shows the critical state lines (CSLs) obtained through the triaxial tests. The slope (λ) and altitude (Γ) of the CSL at 1 kPa for tailings R were found to be 0.063 and 1.130; for tailings B, $\lambda = 0.0454$ and $\Gamma = 0.914$. The critical state friction ratio (M_{tc}) for the two tailings was similar (1.43 for tailings R and 1.48 for tailings B). DSS tests showed a normalised shear strength (S_u/σ'_{vc}) of the order of 0.20 for both tailings (Figure 6(a)) and BE tests showed a similar dependence of the maximum shear modulus (G_{max}) on the mean effective stress (p') (Figure 6(b)): G_{max} at low p' was less than 20 MPa, increasing up to 80 MPa for p' of the order 300 kPa.

Figure 7 shows typical results from the CSS tests on tailings R and B. The figure shows how the tailings lost stiffness in the stress–strain curves and generated excess pore pressures as the shear strain increased, reflecting typical liquefaction behaviour. In total, 20 CSS tests were performed. These were used

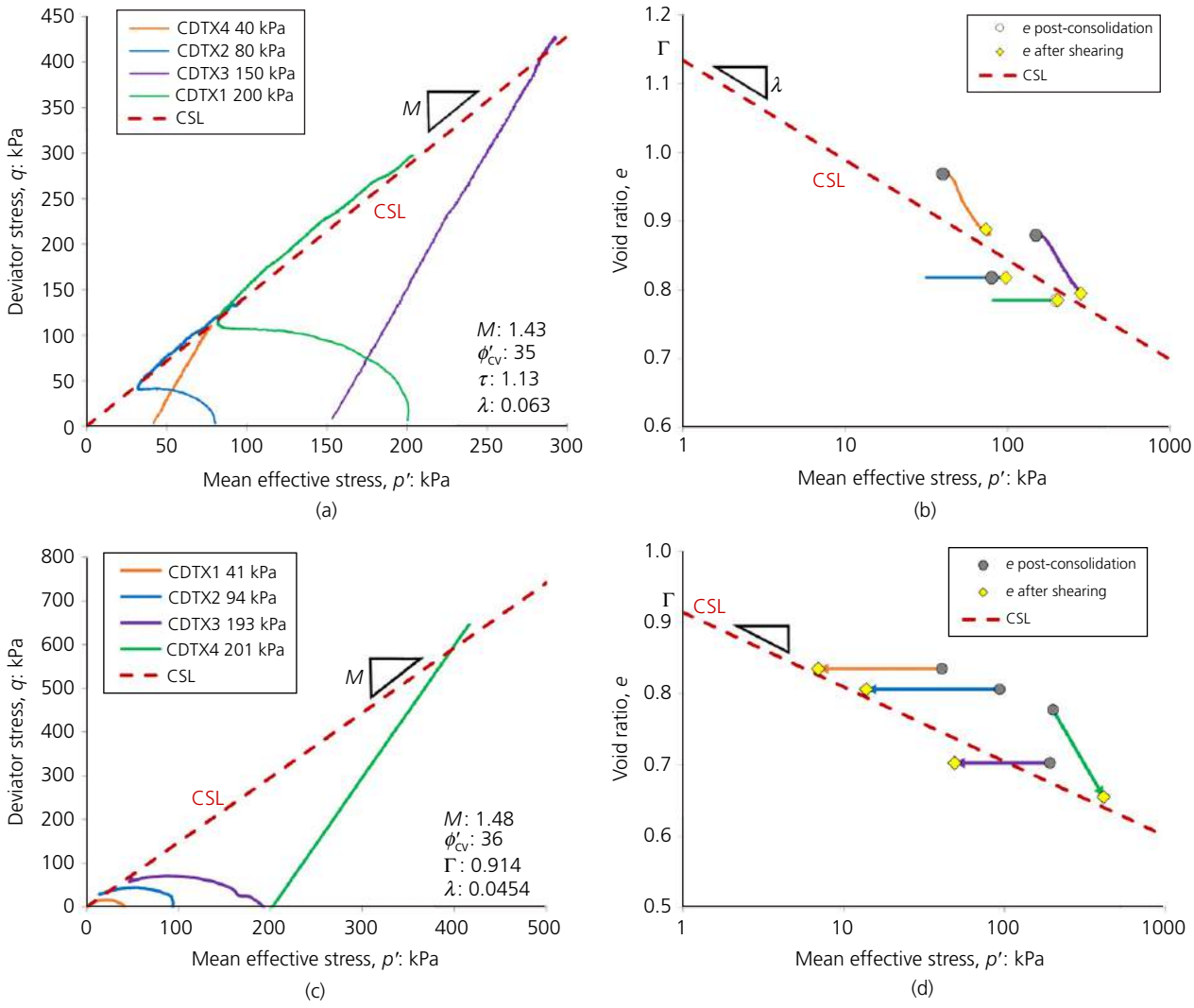

Figure 5. (a) Stress paths and (b) CSL evaluation for tailings R; (c) stress paths and (d) CSL evaluation for tailings B. Γ is the CSL interceptor for 1 kPa in e–ln p' graph; λ is the CSL slope in e–ln p' graph

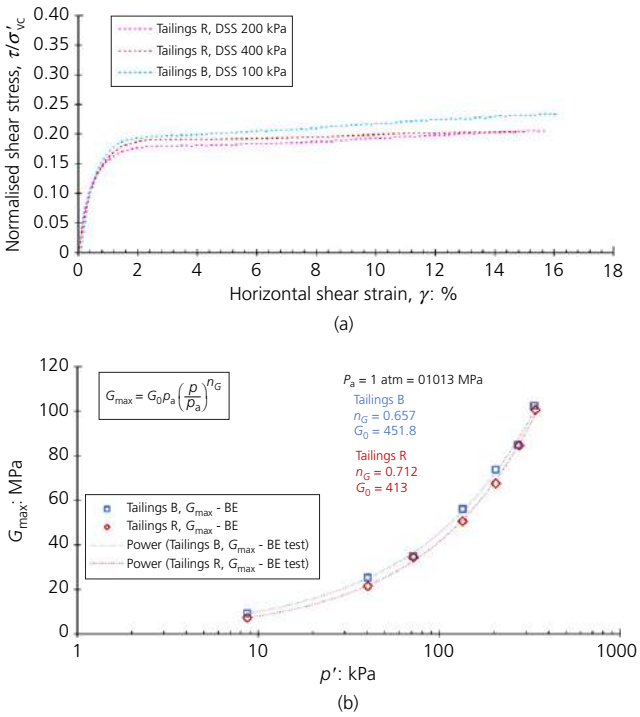

Figure 6. (a) Normalised strength from monotonic shear tests for tailings R and B; (b) G_{max} dependence on p' for mine tailings R and B (evaluated from BE tests)

to define the liquefaction resistance curves (LRCs) and to calibrate the constitutive models, as discussed later in the paper. Figure 8 shows the G/G_{max}–γ and G–γ curves for tailings B and the core material: even though there was a large difference in the G values for the mine tailings and the core materials, the differences in G/G_{max} were in a narrower range. These curves were used for the calibration of the numerical models. Figure 9 shows the results of multichannel analyses of surface waves (MASW) tests performed to characterise the stiffness of the bedrock materials.

5. Numerical model and initial stresses before seismic loading

The dam was modelled using the software FLAC (fast Lagrangian analysis of continua) (ICG, 2019). FLAC is well-suited for performing dynamic analysis and tracking deformations in non-linear materials because it always solves the motion equation in an explicit scheme. Because FLAC is formulated using finite differences, there are no shape functions to capture the variation of field parameters (e.g. displacement, stresses), as in the finite-element method; instead, the derivatives of the governing equations are directly replaced by algebraic finite differences at discrete points in the problem domain. As shown in Figure 10(a), FLAC assumes no interactions between variables within a calculation cycle. For instance, updating stresses (internal variables) does not affect the updating of velocities and displacements (primary

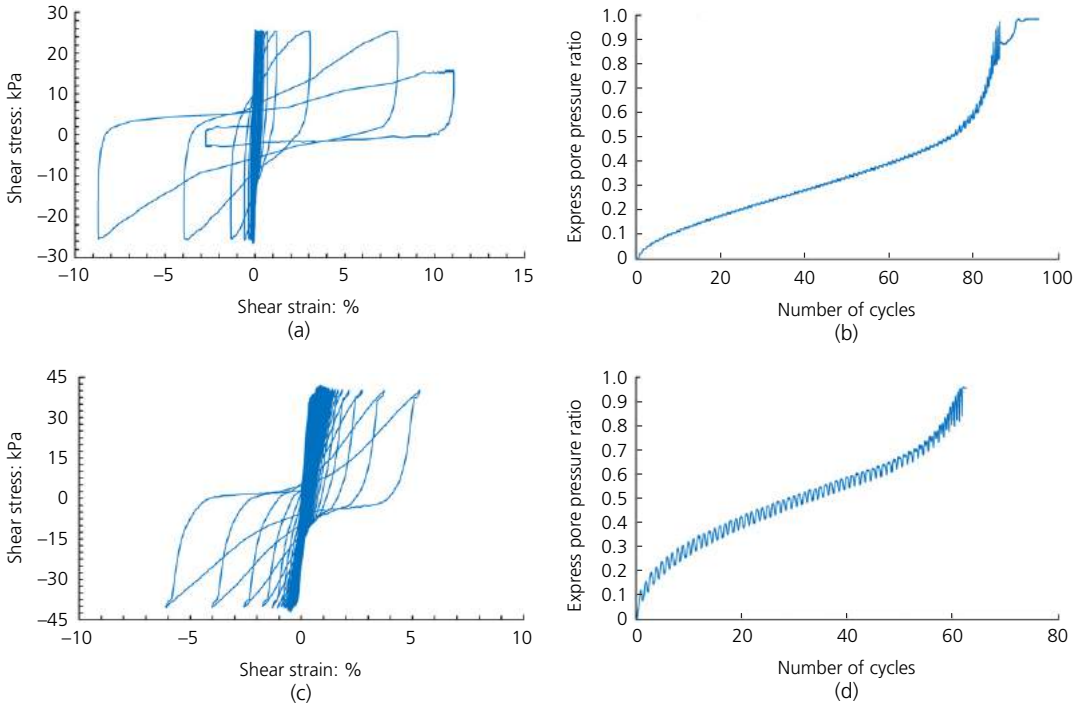

Figure 7. Typical results from cyclic tests on tailings R and B: (a) shear stress–strain response for tailings R (CSR = 0.13, σ_V = 200 kPa); (b) excess pore pressure generation on tailings R (CSR = 0.13, σ_V = 200 kPa); (c) shear stress–strain response for tailings B (CSR = 0.10, σ'_V = 400 kPa); (d) excess pore pressure generation on tailings B (CSR = 0.10, σ'_V = 400 kPa)

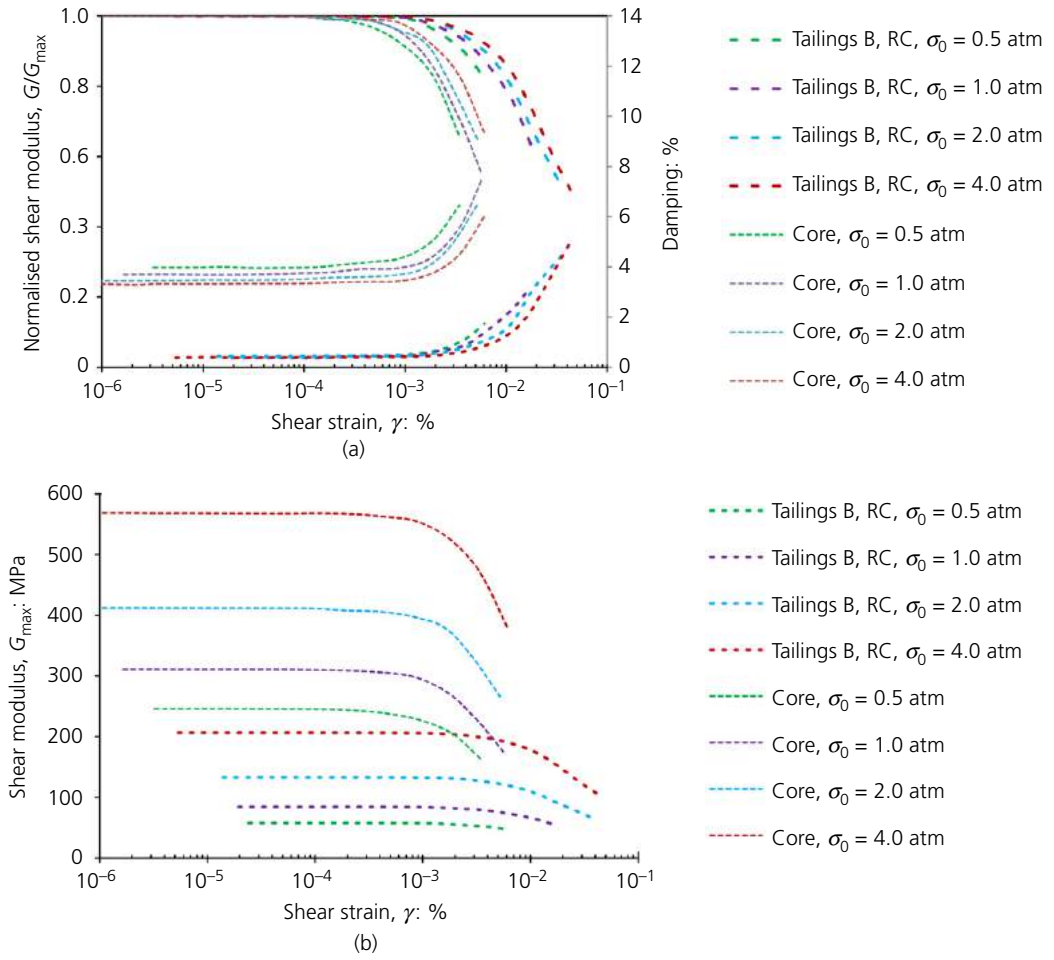

Figure 8. Results from resonant column (RC) tests: (a) G/G_{max} and damping for tailings B and core dam materials; (b) plots of G against shear strain for tailings B and core dam materials (1 atm = 0.1013 MPa)

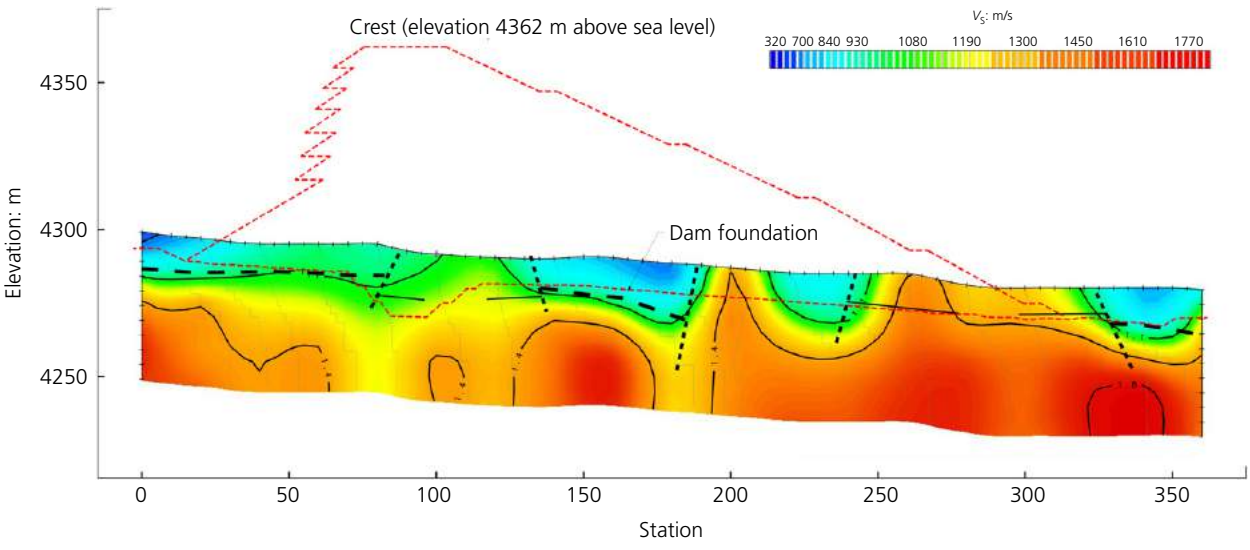

Figure 9. Shear wave velocities (V_s) of bedrock obtained from MASW measurements

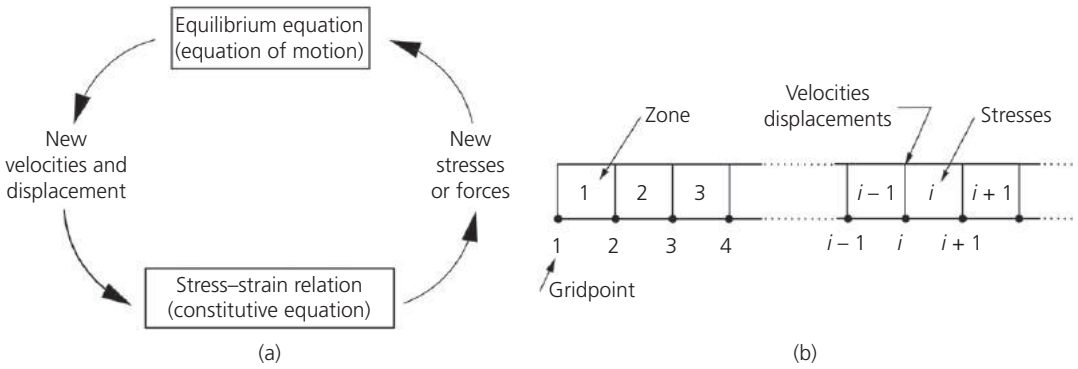

Figure 10. (a) Explicit calculation cycle in FLAC; (b) numbering scheme in FLAC illustrating that the *i*th zone is between gridpoints *i* and *i* + 1. At each FLAC step, the cycle in (a) is applied to the zones and gridpoints in (b) under an explicit scheme

variables). This characteristic requires a small timestep to be selected so that the calculated information from one element cannot physically pass into neighbouring elements. Figure 10(b) shows the numbering scheme for elements and grid points in a bar in FLAC. Additional details on FLAC can be found elsewhere (ICG, 2019). Details of the constitutive model are provided later in the paper.

The FLAC model for the tailings dam is shown in Figure 11. The dimensions of the model and zones satisfy seismic wave transmission requirements according to the recommendations of Kuhlemeyer and Lysmer (1973), which state that the maximum zone dimension should be less than one-tenth to one-eighth of the wavelength associated with the highest frequency of the ground motion. Frequencies larger than 10 Hz were filtered out as these carry a relatively small amount of energy (Mánica *et al.*, 2014); the maximum transmitted frequency was thus 10 Hz. Sensitivity to the considered maximum frequency on the dynamic analyses discussed later was not observed. In addition, considering the minimum shear wave velocity (V_s) in the model to be of the order of 100 m/s (associated with the first metres of the deposited mine tailings), the thickness of the zones in the FLAC model was specified as 1 m ($(1/10) \times (100/10)$). The two displacements in the base and the lateral displacements in the left- and right-hand boundaries were restricted for the static analyses. The dynamic analyses considered quiet boundary conditions for the bottom part of the model, where the input motion was prescribed as a time history of shear stresses, obtained as $\tau = 2V_s\rho V(t)$, where V_s is the shear wave velocity in the bedrock, ρ is the bedrock density and $V(t)$ is the velocity obtained from the outcrop acceleration time history provided from the PSHA. In addition, free-field FLAC boundaries (ICG, 2019) in the left- and right-hand model boundaries were also used during the dynamic analyses. Before performing the dynamic analyses, the dam body and its foundation were analysed under gravitational loads with drained conditions to establish the pre-earthquake stress state. The gravitational loads were applied as part of a staged construction procedure in FLAC.

The Mohr–Coulomb model was used for the tailings and dam materials (with cohesion and friction properties estimated from triaxial tests for similar materials in the area) and the bedrock was modelled as an elastic unit. Bedrock elastic parameters

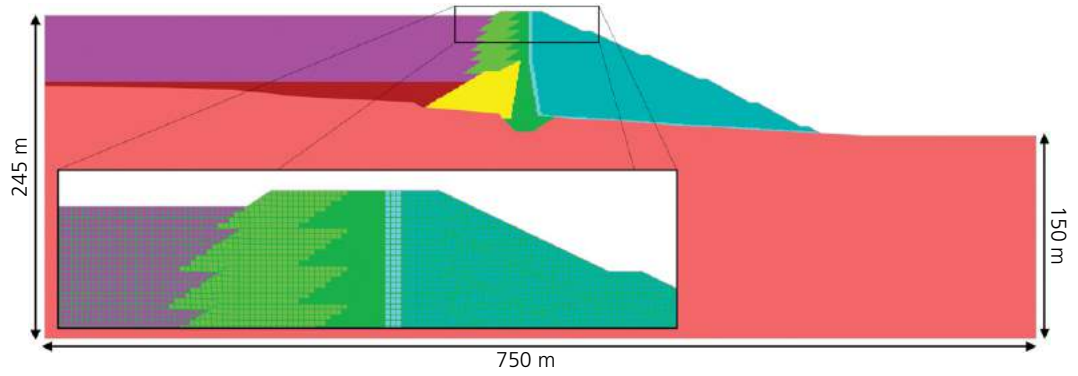

Figure 11. FLAC model for the dam evaluated in this study

Table 1. Material properties for static and flow analyses

	Dry unit weight, γ_{dry}: kN/m^3	Friction angle, ϕ': degrees	Cohesion, c: kPa	Poisson's ratio, ν	Static shear stiffness, G[a]: MPa	Bulk modulus, K[b]: MPa	Porosity, n	Hydraulic conductivity, K: m/s
Structural fill	21.0	38	0	0.35	70	210	0.30	1×10^{-7}
Core	20.0	34	8	0.35	67	200	0.35	1×10^{-7}
Filter/drain	17.0	35	0	0.33	46	120	0.33	2×10^{-3}
Rockfill platform	20.5	40	0	0.30	78	169	0.26	1×10^{-3}
Tailings	14.5	30	0	0.35	3.5	10.5	0.48	1×10^{-7}
Bedrock	25.0	—	—	0.28	382	740	0.15	1×10^{-6}

[a]G was taken as $0.1G_{max}$. The small-strain shear modulus was estimated as $G_{max} = \rho V_s^2 G_{max} = \rho V_s^2$, where ρ is the total density of the material
[b]Bulk modulus was calculated as $K = G2(1 + \nu)/(3(1 - 2\nu))$

were obtained from MASW tests, while the properties of the dam materials were estimated based on the shear wave velocity (V_s) measured from similar materials in the dam area. Groundwater boundary conditions were applied to the model to obtain a water table descending through the filter/drain location and to ensure a saturated condition for the tailings. This represents a critical stability condition for the TSF, which was considered appropriate for the analyses. The specific boundary conditions for the groundwater analyses consisted of fixing the pore pressures using a hydrostatic distribution in the left- and right-hand sides of the model (i.e. the pore pressures were fixed as zero at the surface and increased linearly with depth). In addition, the saturation was fixed as one at the tailings impoundment. The properties considered for the static and groundwater analyses are listed in Table 1. Figure 12 shows the model's initial stress state and the water table location before the dynamic analyses.

6. Dynamic analyses

6.1 Constitutive models and calibrations

The UBCHYST (Naesgaard, 2011) constitutive model was selected for the structural fill, core, filter/drain and rockfill platform materials. These materials were considered to be non-liquefiable due to their high permeability, particle size or degree of compaction. UBCHYST is a two-dimensional, hysteretic soil model formulated to capture the earthquake response of soils in which the generation of excess pore pressures due to cyclic loading is not expected (e.g. highly permeable granular soils). The UBCHYST model uses the Mohr–Coulomb failure criterion, extended with a tangent shear modulus (G_t), which is a function of the stress ratio, the stress ratio since the last reversal (η_{1f}) and the change in stress ratio to reach failure (η_{1f}); it is controlled according to:

$$\text{1a.} \quad G_t = G_{max}\left(1 - \left(\frac{\eta_1}{\eta_{1f}}\right)R_f\right)^n \text{mod1} \cdot \text{mod2}$$

$$\text{1b.} \quad \text{mod2} = 1 - \left|\frac{\eta_{max}}{\eta_f}\right|^{rm} \text{dfac} \geq 0.2$$

For didactic purposes, η_1, η_{1f}, η_{max} and η_f are presented in Figure 13 and n, R_f, mod1, rm and dfac are fitting parameters that are iteratively adjusted to match the shear modulus reduction (G_t/G_{max}) and damping curves. Figure 13 illustrates

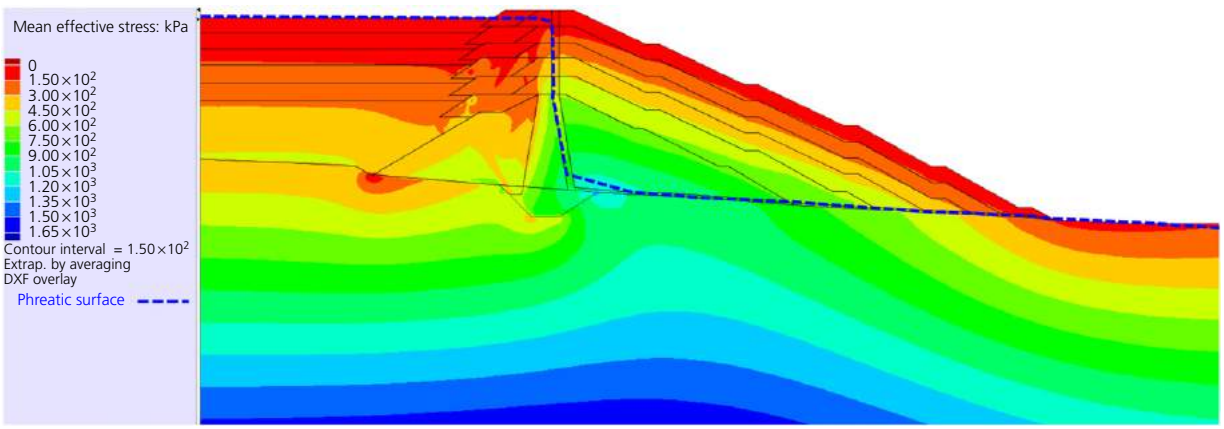

Figure 12. Initial (i.e. before seismic loading) mean effective stress (p') and location of water table

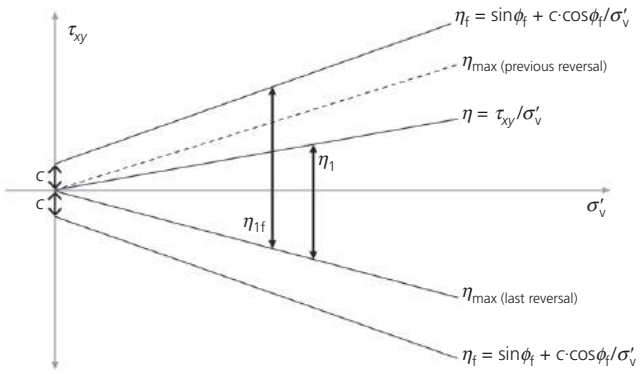

Figure 13. Illustration of how the UBCHYST model controls the scaling of the tangent of the shear modulus to represent a hysteretic behaviour. The parameters used are defined in the notation list

the key parameters that control the scaling of Equation 1. Additional details on the UBCHYST model are provided by Naesgaard (2011). The UBCHYST model was used due to its simplicity yet significant use by geotechnical engineers in the mining industry. The information required to calibrate the model includes the strength properties (i.e. cohesion, friction), stiffness properties (including G_{max} and G_t/G_{max}) and damping curves.

The calibration of parameters for the materials where the UBCHYST model was used is now discussed. In the case of the filter/drain, structural fill and rockfill platform, G_{max} was estimated using shear wave velocity measurements from similar materials in existing dams close to the dam evaluated in this study. G_{max} in the core material was estimated based on resonant column test results previously discussed. The dependence of G_{max} on p' was represented according to Equation 2, proposed by Seed *et al.* (1984):

$$2. \quad G_{max} = 21.7 k_{2,max} P_a \left(\frac{p'}{P_a}\right)^{0.5}$$

where G_{max}, $k_{2,max}$, P_a and p' are, respectively, the small-strain shear modulus, the modulus coefficient, atmospheric pressure and the mean effective stress. A summary of the dam and foundation dynamic properties is provided in Table 2, which shows the $k_{2,max}$ values selected for the different construction materials.

Experimental curves available in the literature and laboratory-based curves were used to calibrate the UBCHYST model using element-level simulations; the UBCHYST parameters were iterated until the numerically simulated G/G_{max} curves reasonably represented the target G/G_{max} curves. The G/G_{max} and damping curves from Rollins *et al.* (1998) and Seed *et al.* (1986) were considered for the rockfill materials. The curves from Darendeli (2001) and Stokoe *et al.* (2004) were considered for the structural fill and the filter/drain materials. G/G_{max} and damping ratio curves for the core material were obtained from resonant column torsional shear (RCTS) tests up to a shear strain of $\sim 1.0 \times 10^{-2}\%$ and complemented by the curves reported by Seed *et al.* (1986). Similarly, G/G_{max} and damping ratio curves for the tailings were obtained from RCTS tests up to a shear strain of $\sim 1.0 \times 10^{-2}$ and complemented by the curves presented by Darendeli (2001) and Vucetic and Dobry (1991). Figure 14 shows comparisons of the G/G_{max} and damping curves calibrated in FLAC and the experimental curves. The strength parameters of the rockfill platform and structural fill for the dynamic analyses were estimated based on data reported by Leps (1970). The parameters selected for the rockfill platform were between the lower bound values and the average values for rockfill materials, whereas the parameters selected for the structural fill were comparable to the lower bound values. The friction angle ϕ was estimated based on the work of Barton and Kjaersnli (1981) using Equation 3:

$$3. \quad \phi = \phi_1 - \Delta\phi \log\left(\frac{\sigma'_3}{P_a}\right)$$

in which σ'_3, ϕ_1 and $\Delta\phi$ are, respectively, the minor principal effective stress, the reference friction angle (at $\sigma'_3 = P_a$) and the friction angle reduction for every log cycle of stress level increase.

The strength parameters and UBCHYST calibrated parameters for the dam materials are presented in Table 3. Calibration parameters for the core and structural fill were

Table 2. Dam and foundation properties for dynamic analysis

	Model	Dry unit weight, γ_{dry}: kN/m^3	Modulus coefficient, $k_{2,max}$	Poisson's ratio, ν	Small-strain shear modulus, G_{max} @ 1 atm: MPa	Bulk modulus, K_{max} @ 1 atm: MPa
Structural fill	UBCHYST	21.0	160	0.35	350	1049
Core	UBCHYST	20.0	140	0.35	308	924
Filter/drain	UBCHYST	17.0	110	0.33	242	631
Rockfill platform	UBCHYST	20.5	180	0.30	396	858
Bedrock	Elastic	25.0	—	0.28	3817	7402

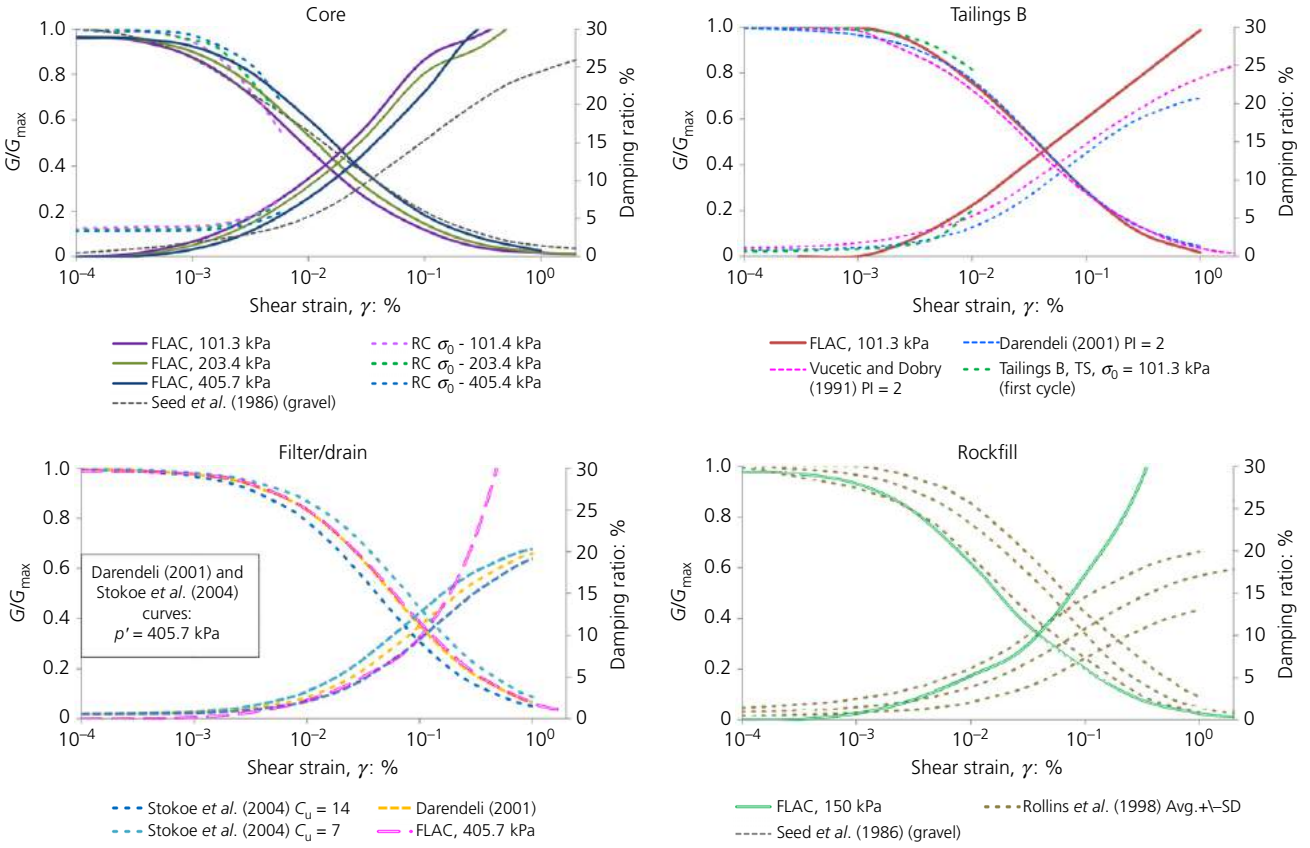

Figure 14. UBCHYST model calibration for the different materials considered in this study (C_u, uniformity coefficient; RC, resonant column; TS, torsional shear

Table 3. Strength parameters and UBCHYST calibration parameters

Material	Friction angle: degrees			Cohesion, c: kPa	Mean effective stress range, p': kPa	UBCHYST calibration parameters				
	ϕ	ϕ_1	$\Delta\phi$			H_n	H_{rf}	H_{rm}	H_{dfac}	H_{dmof1}
Structural fill	Leps (1970)	40	6	0	0–150	2.0	0.98	1	0.7	1
					150–250	2.5				
					250–350	2.7				
					350–450	2.7				
					>450	2.7				
Core	34	—	—	8	0–150	3.0	0.98	1	0.7	1
					150–250	3.5				
					250–350	3.7				
					350–450	3.7				
					>450	3.7				
Filter/drain	35	—	—	0	—	1	0.98	1	0.6	1
Rockfill platform	Leps (1970)	45	6	0	—	2	0.70	1	0.8	1

obtained for specific stress ranges using the resonant column test results.

The constitutive model PM4Silt (Boulanger and Ziotopoulou, 2018b) was selected to represent the response of the tailings materials because they are expected to be susceptible to generating excess pore pressures, as demonstrated through the performed CSS tests. PM4Silt is a stress-ratio-based, critical-state-consistent model formulated under the framework of bounding surface plasticity (Dafalias and Manzari, 2004).

PM4Silt was developed to represent the response of low-plasticity silts and clays to cyclic loadings and is particularly beneficial in geotechnical earthquake engineering applications. The primary input parameters of the PM4Silt constitutive model are the undrained shear strength ratio ($S_{u,cs}/\sigma'_{vc}$) (or undrained shear strength $S_{u,cs}$), the shear modulus coefficient (G_0), the contraction rate parameter (h_{p0}) and an optional post-strong-shaking shear strength reduction factor. The secondary input parameters of the model have default values. Still, they can be set according to the available information for the material being evaluated using information from CSS tests and liquefaction resistance curves (LRCs).

The LRCs (i.e. cyclic stress ratio (CSR) plotted against the number of cycles for liquefaction) obtained from laboratory tests for tailings R and B are shown in Figure 15. Interestingly, the slopes of the LRCs for tailings R and B are flatter (of the order of 0.13) than typical LRCs for sands (i.e. 0.30). In addition, all the CSR values were modest (i.e. not exceeding 0.2). It was also observed that the LRCs do not present an important sensitivity in terms of the confinement stresses before cyclic loading, which contrasts with the behaviour of sands (Idriss and Boulanger, 2008). This behaviour may be associated with the larger compressibility of tailings materials compared with natural sands. To calibrate the PM4Silt model, $S_{u,cs}/\sigma'_{vc}$was estimated from the monotonic shear tests and the bounding surface parameter $n_{b,wet}$ was set to 1.0 in order to limit the peak shear resistance obtained in the simulation, which matched the strain-hardening response observed in the DSS test where peaks were not observed. G_0 and the shear modulus exponent (n_G) values were calculated from the BE tests (Figure 6). The critical state friction angle (ϕ_{cv}) and the slope of the CSL (λ) were obtained from the CSLs; all remaining parameters except h_{p0} were initially assigned default parameters as recommended by Boulanger and Ziotopoulou (2018b). Undrained cyclic loading simulations with uniform CSR were performed in FLAC to calibrate h_{p0} using the experimental LRCs as targets. The stress–strain and stress-path responses in the experiments and the numerical simulations were examined to modify the secondary parameters further. The secondary parameters were modified to flatten the LRC and generate stress–strain and excess pore pressure responses similar to those observed experimentally. A summary of the calibrated PM4Silt parameters after several iterations is provided in Table 4. Figure 15 shows the experimental and numerical calibrated LRCs. Figures 16 and 17 show representative calibrated responses compared against experimental responses for mine tailings R and B. Finally, the bedrock was simulated as an elastic material with a stiffness estimated from the shear wave velocity measurements. A shear wave velocity of 1200 m/s was considered.

7. Results

The seismic response of the tailings dam–foundation system, considering the design ground motion that led to the more conservative results, is discussed in this section. Figure 18 shows the estimated horizontal and vertical displacements. The maximum vertical displacements were found to be of the order of 1.4 m and occurred in the crest area, close to the rockfill platforms. The maximum horizontal displacements occurred in a localised area near the crest and the rockfill platforms and were of the order of 2.75 m. The horizontal displacements in other areas of the rockfill platform in the upstream slope were found to be of the order of 1.00 m and the maximum horizontal displacements in the downstream slope were also of the order of 1.00 m. The filter/drain and core experienced horizontal displacements in the range 0.3–1.0 m in the crest and vertical displacements up to 1.0 m. In practice, these displacements can be used as inputs to check dam integrity using project-specific design criteria. Design often considers

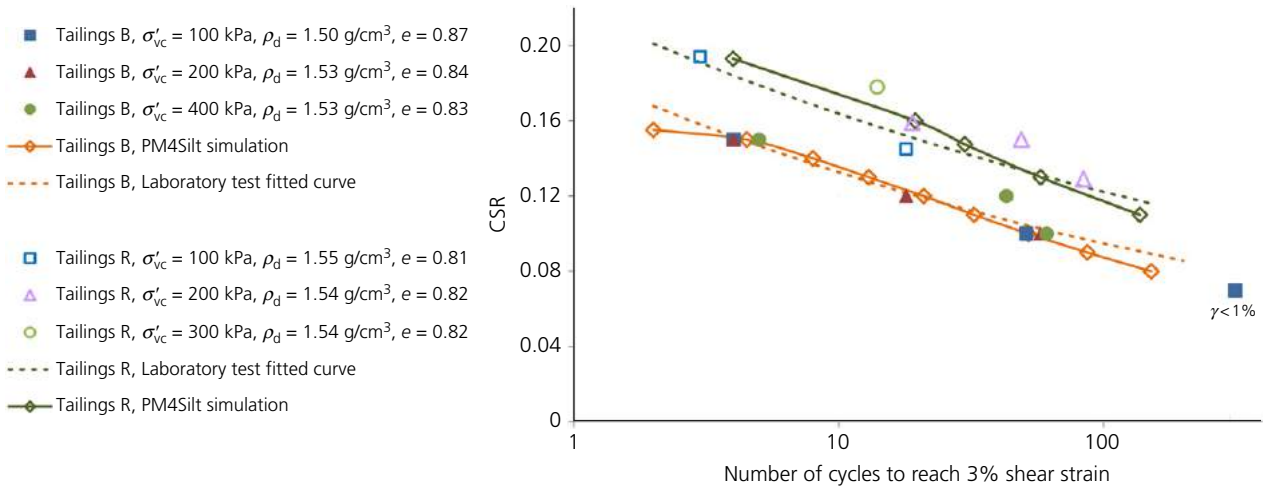

Figure 15. CSR plotted against number of cycles needed to reach 3% shear strain in undrained CSS tests for tailings B and tailings R

Table 4. Input parameters for PM4Silt calibrations for tailings

Input parameters	Default value	Calibration parameters	
		Tailings R	Tailings B
Primary parameters			
Undrained shear strength ratio at critical state, $S_{u,cs}/\sigma'_{vc}$	—	0.2	0.16
Shear modulus coefficient, G_0	—	413	451
Contraction rate parameter, h_{p0}	—	14	6.5
Secondary parameters			
Initial void ratio, e	0.9	0.82	0.98, 0.86[a]
Shear modulus exponent, n_G	0.75	0.712	0.657
Critical state friction angle, ϕ_{cv}	32	35	36
Compressibility in e–ln p' space, λ	0.06	0.063	0.0454
Sets bounding p_{min}, $r_{u,max}$	$p_{min} = p_{cs}/8$	Default	0.98
Bounding surface parameter, $n_{b,wet}$	0.8	1	1
Bounding surface parameter, $n_{b,dry}$	0.5	Default	Default
Dilation surface parameter, n^d	0.3	Default	Default
Dilatancy parameter, A_{d0}	0.8	0.6	Default
Plastic modulus ratio, h_0	0.5	Default	Default
Fabric term, Z_{max}	$10 \leq 40(S_u/\sigma'_{vc}) \leq 20$	80	Default
Fabric growth parameter, c_z	100	75	65
Strain accumulation rate factor, c_ξ	$0.5 \leq (1.2S_u/\sigma'_{vc} + 0.2) \leq 1.3$	0.9	Default
Modulus degradation factor, C_{GD}	3	Default	Default
Plastic modulus factor, $C_{k\alpha f}$	4	Default	Default

[a]0.98 was used for the 10 m of superficial tailings; 0.86 was assigned for deeper tailings

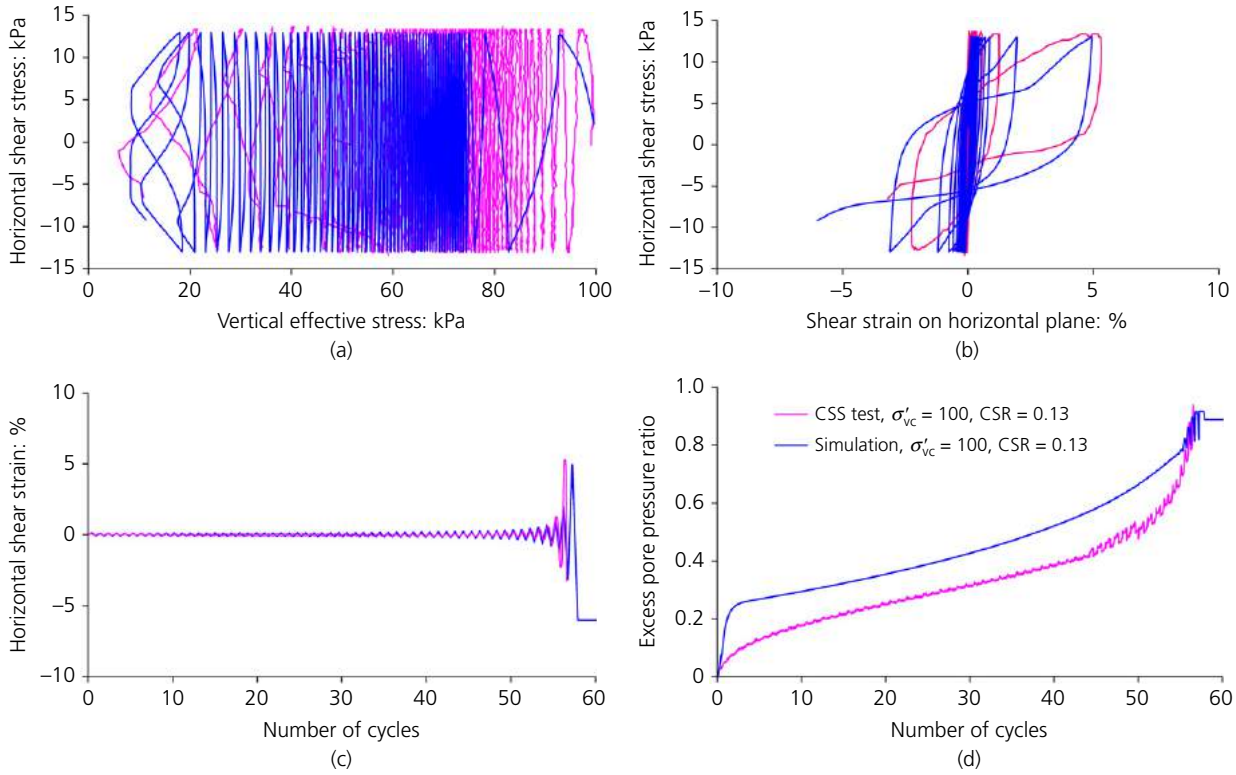

Figure 16. Comparison of calibrated and experimental responses on mine tailings R, considering CSS test with CSR = 0.13 and confinement of 100 kPa

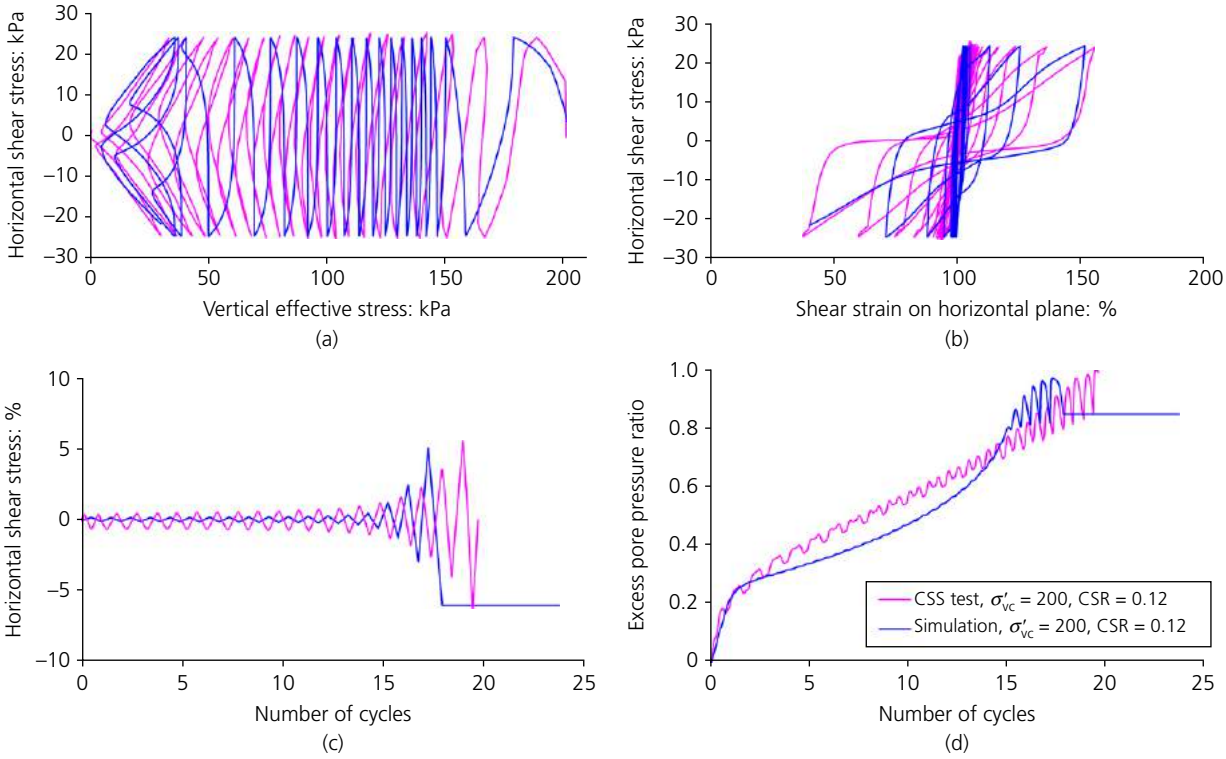

Figure 17. Comparison of calibrated and experimental responses on mine tailings B, considering CSS test with CSR = 0.15 and confinement of 200 kPa

the potential loss of freeboard due to seismically induced settlements (the freeboard is 3 m in this case), the integrity of the drain and filters and displacements in the dam slopes. As illustrated in this study, these parameters can be calculated from non-linear dynamic effective stress analyses and are critical inputs for planning the operation and management of TSFs in seismic areas.

Figure 19 shows the deformed geometry of the dam compared with the geometry before seismic excitation. It can be observed that the area with the highest displacements is the upstream part of the crest. The apparent mechanism is that displacements at the dam crest are caused primarily by an upstream rotation of the top portion of the upstream rockfill platform into the liquefied tailings. It should be noted that the analyses considered that the pond in the tailings deposit is in contact with the upstream crest slope and that the tailings and core material are saturated. These conditions allowed the generation of excess pore pressures, which promoted the generation of shear strains in specific areas inside the core and the upstream slope, resulting in the observed deformation patterns (i.e. Figure 18). Figure 20 shows the time history of representative displacements in the downstream and crest areas, illustrating how displacements steadily accumulate during the seismic excitation. Finally, Figure 21 shows the zones where the maximum excess pore pressure ratio (R_u) (i.e. the seismically induced excess pore pressure (Δu) divided by the initial vertical effective stress (σ'_{v0})) exceeded 0.7 during seismic loading, considering four different times during the excitation (i.e. 10, 25, 40 and 60 s). It can be observed how the liquefied areas grow as the input seismic motion becomes more intense. It is also interesting to see that most of the tailings within a depth of 20 m in the deposit liquefied ($R_u > 0.7$) and the liquefaction depth increased in the areas close to the upstream slope, likely influenced by the shear stresses imposed by the rockfill platform and dam materials on the tailings close to the upstream slope. These results are consistent with the deformation patterns observed in Figure 18. The analyses show that these patterns are highly influenced by the dynamic response and liquefaction of the mine tailings in the deposit, especially those close to the upstream slope.

The deformations and excess pore pressure generation patterns obtained from two other design earthquake ground motions that were also matched to the design response spectrum (Figure 4) were also similar (see the Appendix). However, the maximum deformations in the dam were controlled by the Arias intensity (Arias, 1970) of the design ground motion. The Arias intensity is an informative scalar ground motion intensity measure that simultaneously captures multiple characteristics of a ground motion recording such as amplitude, frequency content and duration. Interested readers can refer to

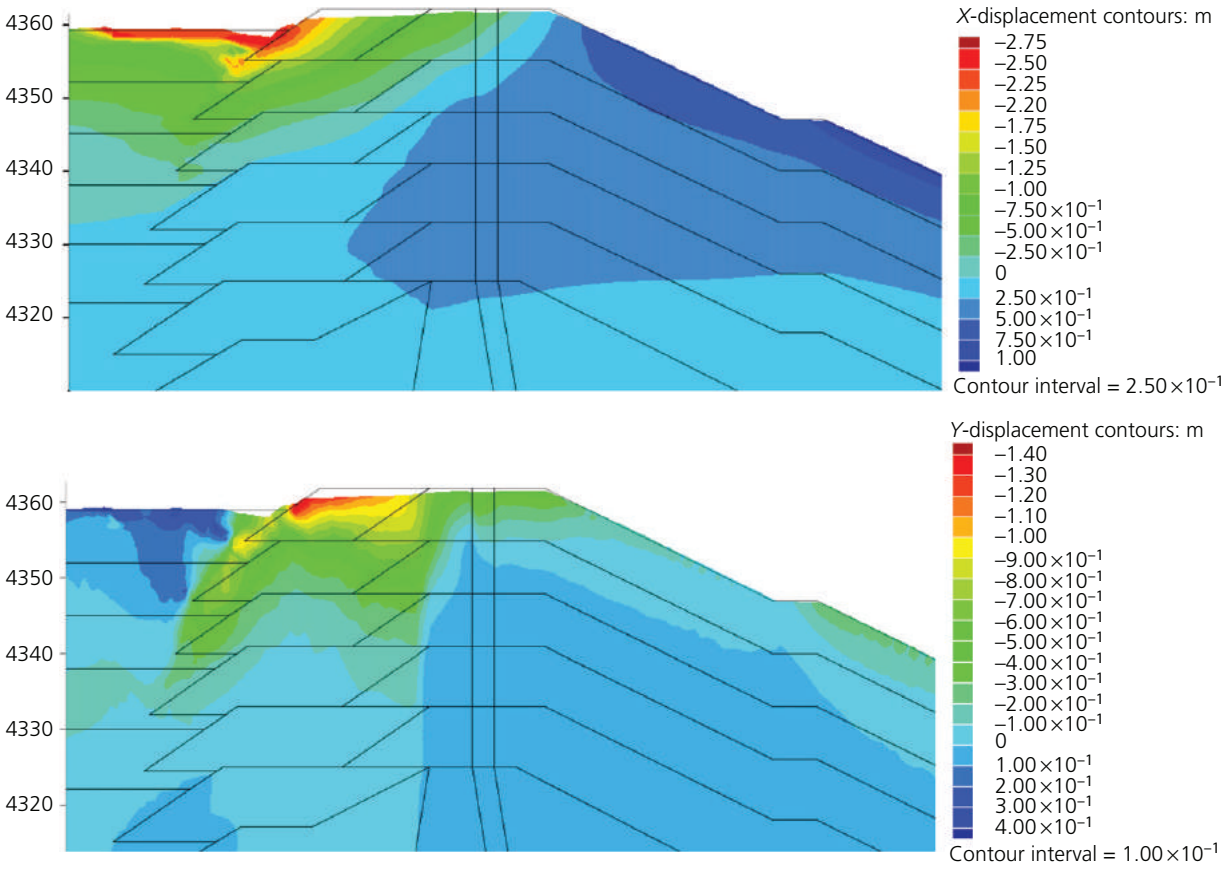

Figure 18. Horizontal (X) and vertical (Y) displacements resulting from dynamic analysis for the MCE design ground motion

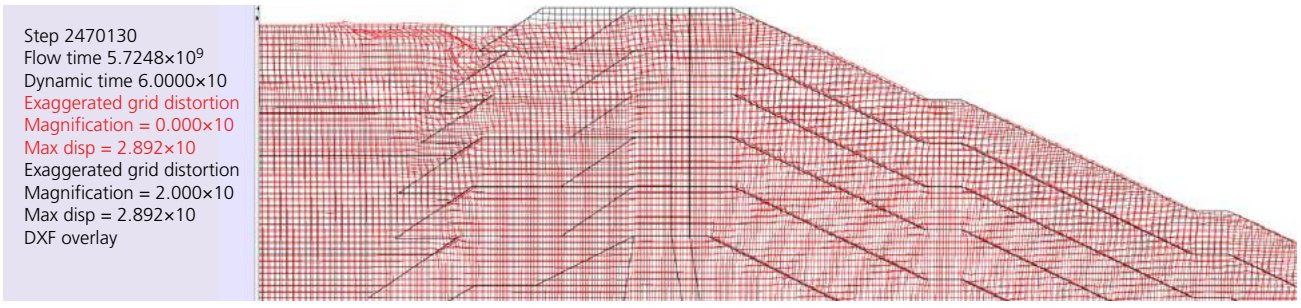

Figure 19. Dam geometry before and after seismic excitation. Notice the deformation patterns in the upstream slope near the crest

Macedo *et al.* (2019), Macedo *et al.* (2021) and Macedo and Liu (2021) for additional details on the Arias intensity. The maximum vertical displacements in the crest area and the maximum horizontal displacements in the downstream slope are plotted against the Arias intensity of the input design ground motions in Figure 22. Interestingly, note how design ground motions 1 and 2, with similar Arias intensities (3.5 and 3.1 m/s), caused similar displacements (vertical displacements of 1.34 and 1.30 m and horizontal displacements of 0.84 and 0.81 m). Notice also how design ground motion 3, with a lower Arias intensity (2.0 m/s), caused lower displacements (i.e. vertical displacement of 0.82 m and horizontal displacement of 0.54 m). These results are consistent with previous studies (e.g. Bray and Macedo, 2017; Bray and Travasarou, 2007; Macedo

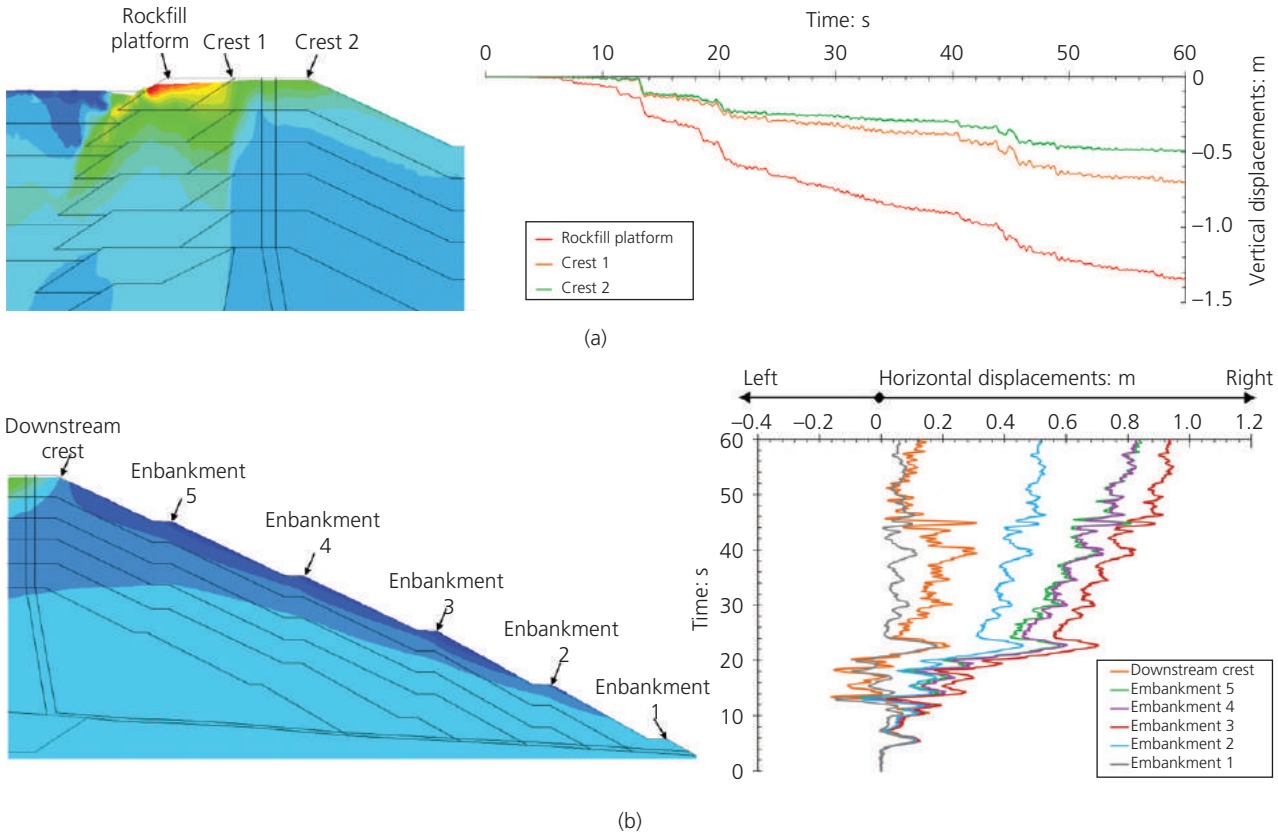

Figure 20. Displacement time histories: (a) vertical displacements in crest area; (b) horizontal displacements in downstream area

et al., 2021; Macedo and Bray, 2018) that highlighted the role of the Arias intensity as a good proxy in explaining seismically induced displacements.

8. Discussion

Four main items related to this study (design earthquakes, the cyclic response of mine tailings, numerical models and fabric effects) are discussed in this section. It is hoped that the following discussions are helpful for future studies related to assessing the seismic performance of TSFs.

8.1 Design earthquakes

As highlighted by Martinez and Hull (2019), even though international guidelines for the seismic analysis and design of water dams and TSFs, such as those issued by the International Commission on Large Dams (Icold, 2010, 2016), the Canadian Dam Association (CDA, 2014), the New Zealand Society on Large Dams (NZ Sold, 2016) and the Australian National Committee on Large Dams (Ancold, 2017), are widely cited by designers, the selection of design earthquake ground motions can often be confusing. For instance, even though the CDA guidelines are commonly used in South America for the 'risk' classification of a TSF (which was also the case in this study), the selection of the design earthquake often relies on local practices. Indeed, the guidelines of Martinez and Hull (2019) considered in this study are based on South American practice during the last decade. This is because the CDA guidelines do not differentiate between the seismic activity of different regions and therefore cannot be directly applied without caution across different tectonic settings. For instance, Canada's seismicity is more stable than the active seismicity in South America; consequently, different criteria (i.e. design earthquakes) should be used in selecting ground motions. The key concept here is that 'large enough' ground motions that allow a 'safe enough' design should be selected. In this context, the practice in South America often considers the MCE 84th percentile for high-risk facilities (i.e. $\varepsilon = 1$; in a PSHA, ε is defined as the number of standard deviations above the mean ground motion intensity measure estimate). However, the fundamental reasons for using the MCE 84th percentile (i.e. $\varepsilon = 1$) have not been assessed for the existing seismicity in South America. Future studies should consider risk-based analyses to evaluate the most suitable design ε in South America, which will likely be region-specific.

8.2 Cyclic response of mine tailings

The relatively 'insensitivity' of the LRCs to changes in the initial confinement for the tailings materials tested in

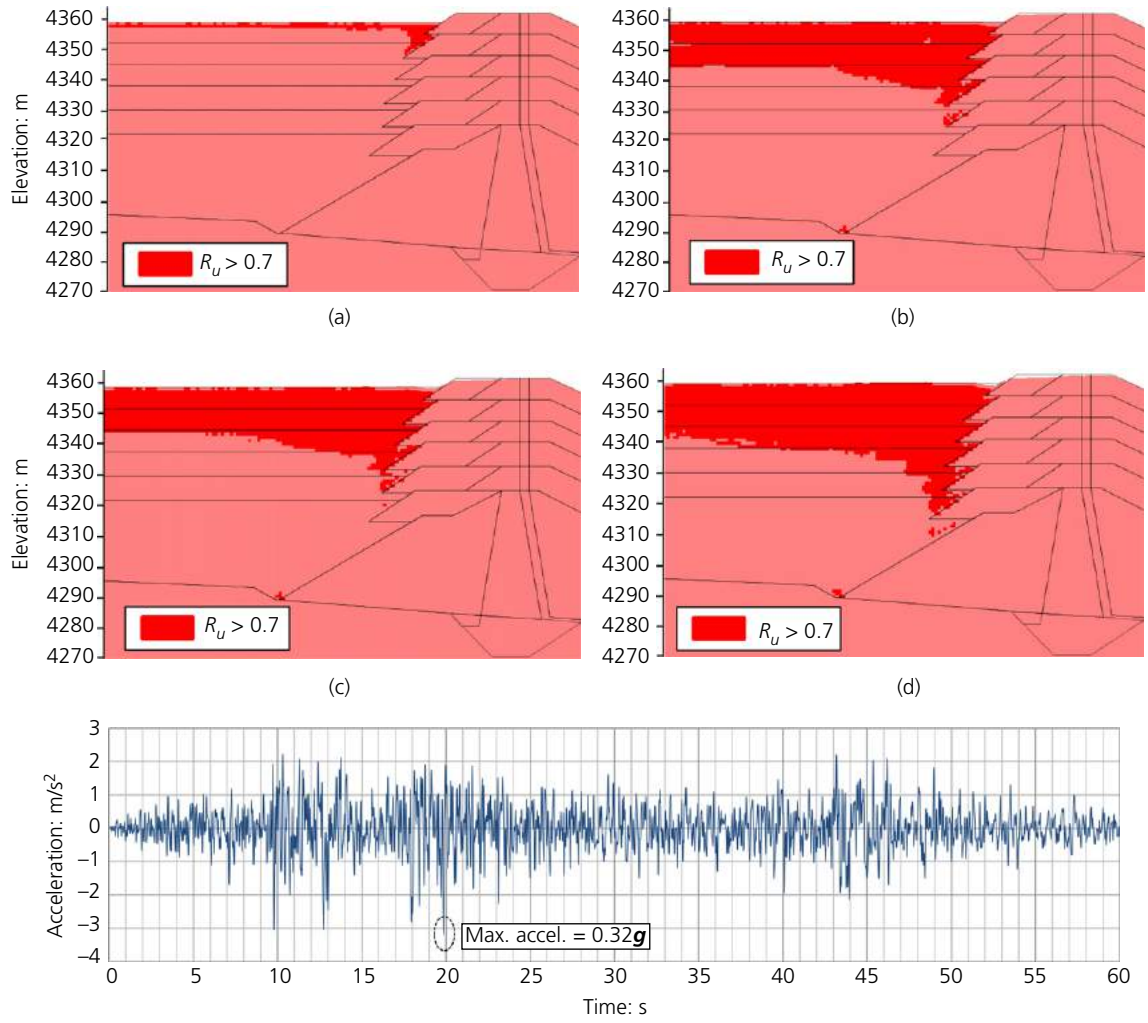

Figure 21. Zones with excess pore water pressure ratio $R_u > 0.7$ at: (a) 10 s; (b) 25 s; (c) 40 s; (d) 60 s. The plot at the bottom of the figure shows the input acceleration time history

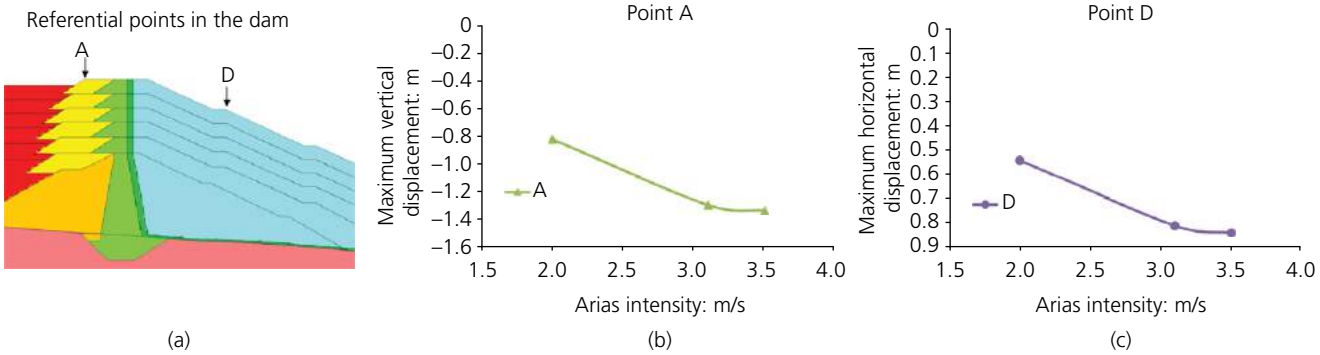

Figure 22. (a) Representative points to track displacements; (b) variation of maximum vertical displacement on point A plotted against the Arias intensity of three design ground motions; (c) variation of maximum horizontal displacement on point D plotted against the Arias intensity of three design ground motions

this study contrasts with what is commonly observed in sands, where the so-called K_σ effect (K_σ is the overburden stress correction factor for liquefaction triggering) provides weaker LRCs with an increase in confinement. In addition, the results from the cyclic tests showed flatter LRCs (i.e. a slope of the order of 0.14) compared with those for sands (typical slopes of the order of 0.33). These observations seem consistent with observations on natural silts (e.g. Oka *et al*., 2018; Wijewickreme *et al*., 2019) and a few previous studies on mine tailings (e.g. Suazo *et al*., 2016; Wijewickreme *et al*., 2005). However, the fundamental reasons underlying these observations are not fully understood. Previous research (Suazo *et al*., 2016; Wijewickreme *et al*., 2005) has suggested two competing mechanisms associated with the increase in the initial confinement before cyclic loading: (*a*) an enhanced contractive response and (*b*) an increase in density. The highlighted behaviours observed in this and previous studies are likely associated with the high compressibility and large critical state stress ratio of tailings. However, more research is warranted to explore this behaviour further. On the other hand, in the context of conventional methods to evaluate liquefaction triggering (e.g. Boulanger and Idriss, 2016), the experimental results suggest a lower K_σ value and a different magnitude scaling factor – influenced by the flatness liquefaction curves – which should be considered when using simplified procedures (e.g. Boulanger and Idriss, 2016) that are part of the current state of practice in TSF projects in South America.

8.3 Numerical models

As part of the initial exploratory analyses performed in this study, the use of constitutive models PM4Sand (Boulanger and Ziotopoulou, 2015) and UBCSand (Byrne *et al*., 2004) for calibrating the LRCs for the mine tailings considered in this study was assessed. These models were unable to capture the slope of the experimentally measured. The PM4Silt model (Boulanger and Ziotopoulou, 2018b), which produced satisfactory calibrations, was thus selected for this research. Future studies should keep evaluating the performance of PM4Silt in representing the cyclic response of mine tailings. The UBCHYST model used in this study to represent the cyclic response of materials that are not expected to generate excess pore pressures follows an extended Masing rule; hence, it tends to overestimate the experiment-based hysteretic damping curves at large strains (e.g. Figure 14). This has been observed for other similar hysteretic models (e.g. Basarah *et al*., 2019; Mánica *et al*., 2014). Basarah *et al*. (2019) evaluated the impact of Masing and non-Masing hysteretic damping on the non-linear dynamic soil–structure interaction analyses of underground excavations, considering results from centrifuge tests. They found that the residuals (i.e. the difference between numerical predictions and centrifuge measurements) of spectral accelerations in the non-Masing models were slightly better for intermediate periods but, in general, the Masing and non-Masing model residuals were comparable. In addition, the non-Masing model was found to provide relatively better performance in terms of comparisons with surface settlements and wall displacements measured in centrifuge tests. However, the performance predicted by the Masing and non-Masing models was not too different (i.e. the predicted settlements/displacements were similar). The authors are not aware of previous works documenting the role of hysteretic models in the seismic response of TSFs. Thus, future studies should explore the implementation and performance of non-Masing models in the dynamic analyses of TSFs.

8.4 Reconstitution of specimens

In this study, the moist tamping technique was used to create reconstituted specimens for evaluating the CSLs of tailings R and B. The selection of this reconstitution method is consistent with the current state of practice in tailings engineering, as reflected in forensic studies on recent worldwide failures (e.g. Morgenstern *et al.*, 2015, 2016, 2019; Robertson *et al.*, 2019). As discussed by Jefferies and Been (2015), the use of moist tamping assumes that the CSL does not depend on the initial fabric. In the case of CSS tests, the slurry deposition technique was used, which has also been used in previous studies on silty soils and mine tailings (e.g. Wijewickreme *et al*., 2005; Donahue *et al*., 2007).

Debate over the ideal method to reconstitute sands, low-plasticity silts and mine tailings to represent in situ fabrics has been underway for decades (e.g. Chang *et al*., 2011; Daliri *et al*., 2015; Høeg *et al*., 2000; Reid and Fanni, 2020). The debate is further complicated by the unknown representativeness of in situ fabric by reconstitution procedures, with only a few efforts attempting to explore this issue on mine tailings (Chang *et al*., 2011, Høeg *et al*., 2000; Reid and Fanni, 2020), which have reported contrasting conclusions. For example, Høeg *et al*. (2000) investigated the differences in the stress–strain responses of gold tailings considering undisturbed, moist tamped and slurry deposited specimens. They found that slurry preparation generally replicated the fabric and behaviour of the undisturbed sample better than moist tamping. In contrast, Reid and Fanni (2020) found that moist tamped specimens, while having a more contractive response compared with undisturbed specimens, reached a similar CSL. Interestingly, the slurry deposited specimens in their study were significantly denser and did not reach critical state conditions but tended towards the same CSL obtained from undisturbed and moist tamped specimens. More research is needed to link the fabric achieved in reconstituted mine tailings specimens for laboratory testing with in situ fabrics. The characterisation of mine tailings properties in this study was based on samples from a pilot plan; the in situ state of the mine tailings is thus not known at this stage. The estimated properties of the mine tailings should be re-evaluated once the tailings are deposited, with a focus on their contractive response. Lastly, due to their deposition, it is likely that mine tailings exhibit a substantial stratigraphic and inherent spatial variability

(see Pua *et al*. (2021) for the definition of variability scales). Future studies should thus also explore the extent of these variabilities.

9. Summary and conclusions

Non-linear dynamic effective stress analyses are increasingly being used in the mining industry to evaluate the seismic performance of critical geotechnical infrastructure such as tailings dams, which are often associated with a potentially high risk. In this context, this paper presented a case study evaluating the seismic response of a centreline tailings dam in the South American Andes affected by subduction earthquakes (interface and intraslab), with a focus on assessing the deformation patterns and evaluating the expected median seismically induced displacements. Boulanger and Ziotopoulou (2018a) discussed the role of non-linear dynamic analyses in the design of geotechnical structures. They recommended the documentation of such studies so that they can be used not only as a reference but also to set a standard for future studies. The aim of this article was to serve that purpose by contributing to the literature of well-documented case studies, which is particularly important for designing TSFs in areas of high seismicity such as South America.

Comprehensive characterisation of the mine tailings was conducted as their response is expected to have a significant effect on the overall response of the dam. This characterisation was used to provide inputs to the PM4Silt constitutive model, which was used to represent the cyclic responses of the mine tailings. Interestingly, the slopes of the LRCs for the mine tailings considered in this study were quite flat compared with those of natural sands. In addition, it was found that confinement did not introduce a significant variation in the cyclic resistance, which is also in contrast to what is commonly observed in sands. These effects may be associated with the larger compressibility of tailings materials and should be investigated further. Moreover, the properties for the mine tailings examined in this study were based on samples from a pilot processing plant. These properties should thus be reassessed once the tailings are deposited in the TSF. In general, the cyclic resistance obtained from CSS tests was relatively modest (the CSR that causes liquefaction was lower than 0.20 in all cases), consistent with the flatness of the LRCs. The modest CSR values are likely influenced by the fine-grained nature of the mine tailings, which is consistent with previous findings on natural silts (e.g. Oka *et al*., 2018). Interestingly, both BE and resonant column tests revealed that G_{max} in the tested mine tailings had a similar dependence on confinement as observed in sands (i.e. a power law captured the increase of G_{max} with confinement). The dynamic properties of the tailings were evaluated through resonant column tests, which showed the typical degradation of G_{max} with shear strain; in particular, the G/G_{max} and damping curves were generally consistent with those reported by Vucetic and Dobry (1991) and Darendeli (2001) for a low PI, as illustrated in Figure 14. Triaxial tests were used to evaluate the CSL. These tests revealed that the critical state stress ratio for the tested tailings was significantly larger (1.43–1.48) than that commonly found for sands (1.2–1.3), which is likely associated with the angularity in tailings materials due to their processing. Finally, it was observed that the shear strength from monotonic shear tests performed on the tailings R materials could be normalised.

For the other materials that are not expected to generate excess pore pressures under cyclic loading, the UBCHYST model (Naesgaard, 2011) was used. The UBCHYST model calibration was based on G/G_{max} and damping curves. Resonant column tests were performed to characterise the G/G_{max} and damping curves of the dam core materials and experimental curves from the literature were used to calibrate other materials in the dam that are not expected to generate excess pore pressures.

The dynamic analyses showed that the seismic response of the mine tailings is critical for the overall response of the dam. In fact, the deformation patterns at the dam crest, associated with an upstream rotation of the top portion of the upstream rockfill platform, were significantly influenced by the liquefaction of mine tailings close to the upstream dam slope. These deformation patterns could not have been evaluated using simplified approaches that are often used in practice (e.g. analyses based on Newmark-based methods (e.g. Bray and Macedo, 2019; Bray *et al*., 2018; Macedo *et al*., 2017)), illustrating the value of performing non-linear dynamic analyses. It was also observed that the Arias intensity of the input ground motions correlated well with the estimated seismically induced displacement, consistent with previous studies.

It is important to reiterate that these analyses were based on samples from a pilot plant; the in situ state of the mine tailings is thus not known at this stage. The estimated properties for the mine tailings should be re-evaluated once the tailings are deposited, with a focus on their contractive response. Moreover, the focus of this study was on assessing the seismic response of the TSF. Further integration of the static (e.g. static liquefaction) and dynamic (e.g. cyclic liquefaction) responses should be performed in the future, once the properties of the as-deposited tailings become available.

Acknowledgement

We thank Mr Ruben Vargas from Knight Piésold Consultores for providing valuable comments for this study.

Appendix

The horizontal displacements and excess pore pressure generation patterns obtained from two other design earthquake ground motions were similar, as shown in Figures 23–26.

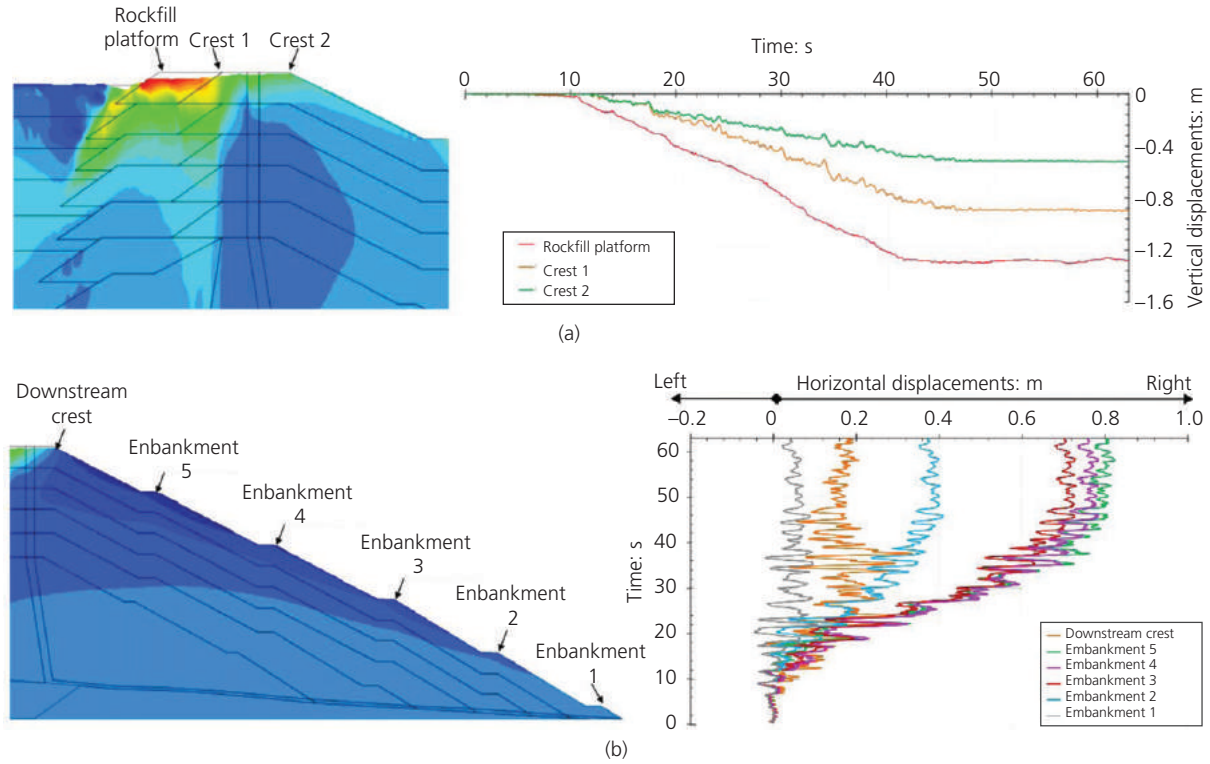

Figure 23. Displacement time histories for design ground motion 2 (Arias intensity of 3.1 m/s): (a) vertical displacements in crest area; (b) horizontal displacements in downstream area

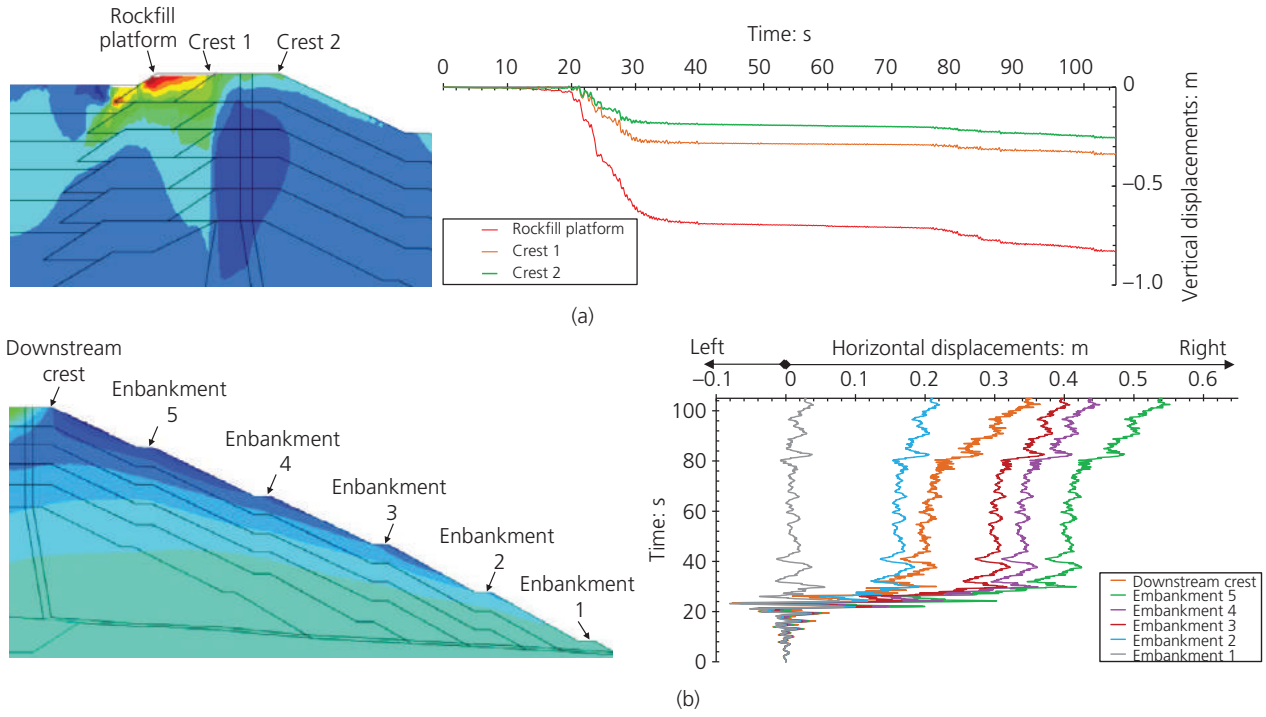

Figure 24. Displacement time histories for design ground motion 3 (Arias intensity of 2.0 m/s): (a) vertical displacements in crest area; (b) horizontal displacements in downstream area

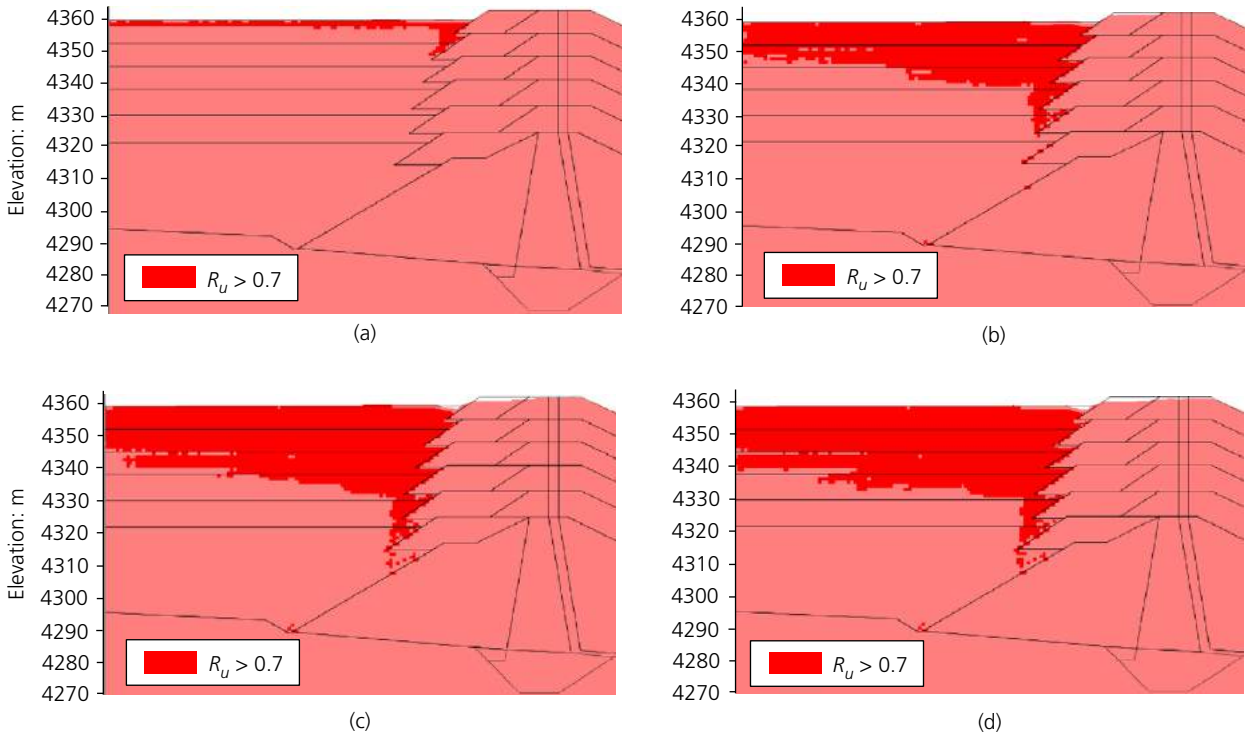

Figure 25. Zones with excess pore water pressure ratio $R_u > 0.7$ at (a) 10 s; (b) 25 s; (c) 40 s and (d) 63 s for design ground motion 2 (Arias intensity of 3.1 m/s)

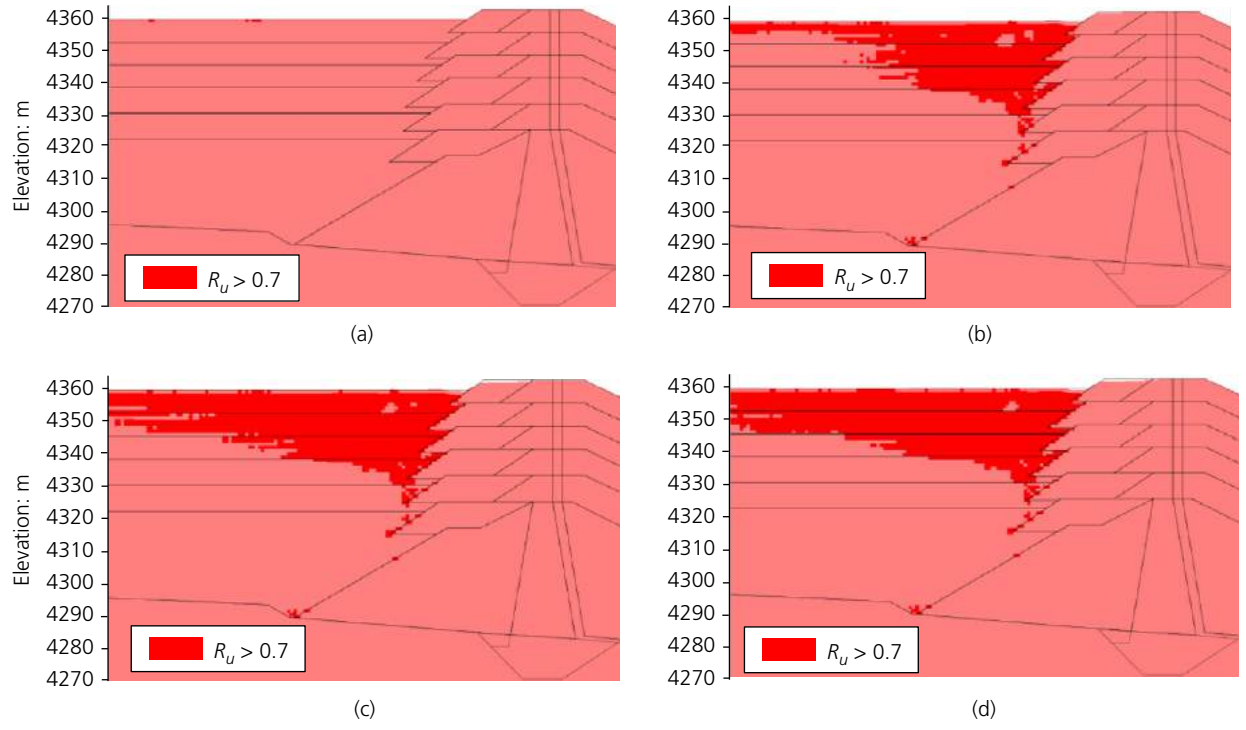

Figure 26. Zones with excess pore water pressure ratio $R_u > 0.7$ at (a) 10 s; (b) 25 s; (c) 50 s and (d) 105 s for design ground motion 3 (Arias intensity of 2.0 m/s)

REFERENCES

Al Atik L and Abrahamson N (2010) An improved method for nonstationary spectral matching. *Earthquake Spectra* **26(3)**: 601–617, https://doi.org/10.1193/1.3459159.

Ancold (Australian National Committee on Large Dams) (2017) *Guidelines for Design of Dams and Appurtenant Structures for Earthquake*. Ancold, Hobart, Tasmania.

Arias A (1970) A measure of earthquake intensity. *Seismic Design for Nuclear Power Plants*. Massachusetts Institute of Technology, Cambridge, MA, USA.

Barton N and Kjaersnli B (1981) Shear strength of rockfill. *Journal of the Geotechnical Engineering Division* **107(GT7)**: 873–891.

Basarah YI, Numanoglu OA, Hashash YM and Dashti S (2019) Impact of hysteretic damping on nonlinear dynamic soil-underground structure-structure interaction analyses. In *Geo-Congress 2019: Earthquake Engineering and Soil Dynamics*. ASCE, Reston, VA, USA, pp. 208–218.

Boulanger RW and Idriss IM (2016) CPT-based liquefaction triggering procedure. *Journal of Geotechnical and Geoenvironmental Engineering* **142(2)**: 04015065.

Boulanger RW and Ziotopoulou K (2015) *PM4Sand (Version 3): A Sand Plasticity Model for Earthquake Engineering Applications*. Center for Geotechnical Modeling, University of California, Davis, CA, USA, Report No. UCD/CGM-15/01.

Boulanger RW and Ziotopoulou K (2018a) On NDA practices for evaluating liquefaction effects. In *Geotechnical Earthquake Engineering and Soil Dynamics V* (Brandenberg SJ and Manzari MT (eds)). ASCE, Reston, VA, USA, GSP 290, pp. 1–20.

Boulanger RW and Ziotopoulou K (2018b) *PM4Silt (Version 1): A Silt Plasticity Model for Earthquake Engineering Applications*. Center for Geotechnical Modeling, University of California, Davis, CA, USA, Report No. UCD/CGM-18/01.

Bozorgnia Y, Abrahamson N, Ahdi SK *et al.* (2021) Next generation attenuation-subduction research program. *Earthquake Spectra*, https://doi.org/10.1177/87552930211056081.

Bray JD and Macedo J (2017) 6th Ishihara lecture: simplified procedure for estimating liquefaction-induced building settlement. *Soil Dynamics and Earthquake Engineering* **102**: 215–231.

Bray JD and Macedo J (2019) Procedure for estimating shear-induced seismic slope displacement for Shallow crustal earthquakes. *Journal of Geotechnical and Geoenvironmental Engineering* **145(12)**: 04019106.

Bray JD and Travasarou T (2007) Simplified procedure for estimating earthquake-induced deviatoric slope displacements. *Journal of Geotechnical and Geoenvironmental Engineering* **133(4)**: 381–392.

Bray JD, Macedo J and Travasarou T (2018) Simplified procedure for estimating seismic slope displacements for subduction zone earthquakes. *Journal of Geotechnical and Geoenvironmental Engineering* **144(3)**: 04017124.

Byrne PM, Park SS, Beaty M *et al.* (2004) Numerical modeling of liquefaction and comparison with centrifuge tests. *Canadian Geotechnical Journal* **41(2)**: 193–211.

Candia G, Macedo J and Magna-Verdugo C (2018) An integrated platform for seismic hazard evaluation. In *Proceedings of the 11th US National Conference on Earthquake Engineering, Los Angeles, CA, USA,*

Candia G, Macedo J, Jaimes MA and Magna-Verdugo C (2019) A new state-of-the-art platform for probabilistic and deterministic seismic hazard assessment. *Seismological Research Letters* **90(6)**: 2262–2275.

CDA (Canadian Dam Association) (2014) *Application of Dam Safety Guidelines to Mining Dams*. CDA, Markham, ON, Canada.

Chang N, Heymann G and Clayton C (2011) The effect of fabric on the behaviour of gold tailings. *Géotechnique* **61(3)**: 187–197, https://doi.org/10.1680/geot.9.P.066.

Dafalias Y and Manzari MT (2004) Simple plasticity sand model accounting for fabric change effects. *Journal of Engineering Mechanics ASCE* **130(6)**: 622–634.

Daliri F, Simms P and Sivathayalan S (2015) Discussion of 'Stiffness and strength governing the static liquefaction of tailings' by F. Schnaid, J. Bedin, AJP Viana da Fonseca, and L. de Moura Costa Filho. *Journal of Geotechnical and Geoenvironmental Engineering* **141(9)**: 07015023.

Darendeli MB (2001) *Development of a New Family of Normalized Modulus Reduction and Material Damping Curves*. PhD dissertation, University of Texas, Austin, TX, USA.

Donahue JL, Bray JD and Riemer MF (2007) Liquefaction Testing of Fine-Grained Soil Prepared Using Slurry Deposition. In *Proceedings 4th International Conference Earthquake Geotechnical Engineering*, paper no. 1226.

Høeg K, Dyvik R and Sandbaekken G (2000) Strength of undisturbed versus reconstituted silt and silty sand specimens. *Journal of Geotechnical and Geoenvironmental Engineering* **126(7)**: 606–617.

ICG (Itasca Consulting Group, Inc.) (2019) *FLAC 8.0 (Fast Lagrangian Analysis of Continua) User Manual*. ICG, Minneapolis, MN, USA.

Icold (2010) *Bulletin 72: Selecting Seismic Parameters for Large Dams: Guidelines, Committee on Seismic Aspects of Dam Design*. Icold, Paris, France.

Icold (2016) *Bulletin 148: Selecting Seismic Parameters for Large Dams. Guidelines, Committee on Seismic Aspects of Dam Design*. Icold, Paris, France.

Idriss IM and Boulanger RW (2008) *Soil Liquefaction During Earthquakes*. Earthquake Engineering Research Institute, Oakland, CA, USA.

Jefferies M and Been K (2015) *Soil Liquefaction: A Critical State Approach*. CRC Press, Boca Raton, FL, USA.

Kuhlemeyer RL and Lysmer J (1973) Finite element method accuracy for wave propagation problems. *Journal of the Soil Mechanics and Foundations Division* **99(5)**: 421–427.

Leps TM (1970) Review of shearing strength of rockfill. *Journal of the Soil Mechanics and Foundation Division* **96(4)**: 1159–1170.

Macedo J and Bray JD (2018) Key trends in liquefaction-induced building settlement. *Journal of Geotechnical and Geoenvironmental Engineering* **144(11)**: 04018076.

Macedo J and Candia G (2020) Performance-based assessment of the seismic pseudo-static coefficient used in slope stability analysis. *Soil Dynamics and Earthquake Engineering* **133**: 106109.

Macedo J and Liu C (2021) Ground-motion intensity measure correlations on interface and intraslab subduction zone earthquakes using the NGA-Sub database. *Bulletin of the Seismological Society of America* **111(3)**: 1529–1541.

Macedo J and Vergaray L (2021) Properties of mine tailings for static liquefaction assessment. *Canadian Geotechnical Journal*, https://doi.org/10.1139/cgj-2020-0600.

Macedo J, Bray J and Travasarou T (2017) Simplified procedure for estimating seismic slope displacements in subduction zones. In *Proceedings of the 16th World Conference on Earthquake Engineering, Santiago, Chile.*

Macedo J, Abrahamson N and Bray JD (2019) Arias intensity conditional scaling ground-motion models for subduction zones. *Bulletin of the Seismological Society of America* **109(4)**: 1343–1357.

Macedo J, Candia G, Lacour M and Liu C (2020) New developments for the performance-based assessment of seismically-induced slope displacements. *Engineering Geology* **277**: 105786.

Macedo J, Abrahamson N and Liu C (2021) New scenario-based cumulative absolute velocity models for shallow crustal tectonic settings. *Bulletin of the Seismological Society of America* **111(1)**: 157–172.

Mánica M, Ovando E and Botero E (2014) Assessment of damping models in FLAC. *Computers and Geotechnics* **59**: 12–20.

Martinez M and Hull A (2019) Toward a common practice in the selection of earthquake ground motion criteria for the design of critical mining facilities at closure and post-closure. In *Mine Closure 2019: Proceedings of the 13th International Conference on Mine Closure* (Fourie AB and Tibbett M (eds)). Australian Centre for Geomechanics, Perth, Australia, pp. 249–262, https://doi.org/10.36487/ACG_rep/1915_20_Martinez.

Morgenstern NR, Vick SG and van Zyl D (2015) *Report on Mount Polley Tailings Storage Facility Breach. Report of Independent Expert Engineering Investigation and Review Panel for the Government of British Columbia and the Williams Lake and Soda Creek Indian Bands.* Province of British Columbia, Victoria, Canada. See www.mountpolleyreviewpanel.ca/final-report (accessed 22/03/2022).

Morgenstern NR, Vick SG, Viotti CB and Watts BD (2016) *Fundão Tailings Dam Review Panel: Report on the Immediate Causes of the Failure of the Fundão Dam.* Cleary Gottlieb Steen & Hamilton LLP, New York, NY, USA.

Morgenstern NR, Jefferies M, Zyl D and Wates J (2019) *Independent Technical Review Board. Report on NTSF Embankment Failure.* Ashurst Australia. See https://www.newcrest.com/sites/default/files/2019-10/190417_Report%20on%20NTSF%20Embankment%20Failure%20at%20Cadia%20for%20Ashurst.pdf (accessed 22/03/2022).

Naesgaard E (2011) *A Hybrid Effective Stress-Total Stress Procedure for Analyzing Embankments Subjected to Potential Liquefaction and Flow.* PhD thesis, The University of British Columbia, Vancouver, BC, Canada.

NZ Sold (New Zealand Society on Large Dams) (2016) *Dam Safety Guidelines.* NZ Sold, Wellington, New Zealand.

Oka LG, Dewoolkar M and Olson SM (2018) Comparing laboratory-based liquefaction resistance of a sand with non-plastic fines with shear wave velocity-based field case histories. *Soil Dynamics and Earthquake Engineering* **113**: 162–173.

Pua LM, Macedo J, Villacreses JP, Caicedo B and Yépez F (2021) A homogenization approach to estimate the shear modulus of spatially variable soil materials. *Soil Dynamics and Earthquake Engineering* **151**: 106970.

Reid D and Fanni R (2020) A comparison of intact and reconstituted samples of a silt tailings. *Géotechnique* **72(2)**: 176–188, https://doi.org/10.1680/jgeot.20.P.020.

Robertson PK, De Melo L, Williams DJ and Wilson GW (2019) *Report of the Expert Panel on the Technical Causes of the Failure of Feijão Dam I.* See http://www.b1technicalinvestigation.com/ (accessed 22/03/2022).

Rollins KM, Evans MD, Diehl NB and Daily WD III (1998) Shear modulus and damping relationships for gravels. *Journal of Geotechnical and Geoenvironmental Engineering* **124(5)**: 396–405.

Seed H and Idriss I (1970) *Soil Moduli and Damping Factors for Dynamic Response Analysis.* Earthquake Engineering Research Centre, Berkeley, CA, USA, Report No. EERC 70-10.

Seed HB, Wong RT, Idriss IM and Tokimatsu K (1984) *Moduli and Damping Factors for Dynamic Analyses of Cohesionless Soils.* Earthquake Engineering Research Center, University of California, Berkeley, CA, USA, Report No. EERC 84-14.

Seed HB, Wong RT, Idriss IM and Tokimatsu K (1986) Moduli and damping factors for dynamic analyses of cohesionless soils. *Journal of Geotechnical Engineering* **112(11)**: 1016–1032.

Stokoe KH, Darendeli MB, Gilbert RB, Menq FY and Choi WK (2004) Development of a new family of normalized modulus reduction and material damping curves. In *Proceedings, NSF/PEER International Workshop on Uncertainties in Nonlinear Soil Properties and their Impact on Modeling Dynamic Soil Response.* University of California at Berkeley, Berkeley, CA, USA.

Suazo G, Fourie A, Doherty J and Hasan A (2016) Effects of confining stress, density and initial static shear stress on the cyclic shear response of fine-grained unclassified tailings. *Géotechnique* **66(5)**: 401–412, https://doi.org/10.1680/jgeot.15.P.032.

Vucetic M and Dobry R (1991) Effect of soil plasticity on cyclic response. *Journal of Geotechnical Engineering* **117(1)**: 89–107.

Wijewickreme D, Sanin MV and Greenaway GR (2005) Cyclic shear response of fine-grained mine tailings. *Canadian Geotechnical Journal* **42(5)**: 1408–1421.

Wijewickreme D, Soysa A and Verma P (2019) Response of natural fine-grained soils for seismic design practice: a collection of research findings from British Columbia, Canada. *Soil Dynamics and Earthquake Engineering* **124**: 280–296.

How can you contribute?

To discuss this paper, please email up to 500 words to the editor at journals@ice.org.uk. Your contribution will be forwarded to the author(s) for a reply and, if considered appropriate by the editorial board, it will be published as discussion in a future issue of the journal.

Proceedings journals rely entirely on contributions from the civil engineering profession (and allied disciplines). Information about how to submit your paper online is available at www.icevirtuallibrary.com/page/authors, where you will also find detailed author guidelines.